Chapter 9

On the admissibility of intermediate shocks

9.1 Introduction

In this Chapter we discuss the admissibility of intermediate shocks in MHD. In Sec. 3.3 we have reviewed the various types of MHD discontinuities which are allowed by the MHD Rankine-Hugoniot (RH) relations. Not all types of MHD discontinuities allowed by the RH relations can arise in MHD flows, however. A clear example are the so-called *expansion shocks*, which take fluid elements from a high-entropy state to a low-entropy state. Expansion shocks are perfectly allowed by the RH relations and are weak solutions of the ideal MHD equations, but they cannot exist in ideal MHD flows because they cannot be formed through wave steepening and because they would disintegrate immediately upon even the smallest perturbation. Another way to see that expansion shocks cannot exist is that they violate the second law of thermodynamics. Such improper shock solutions of the equations are called *inadmissible* shocks, as opposed to *admissible* shocks which can arise in flow solutions.

The hydrodynamic (HD) equations are strictly hyperbolic — wave speeds do not coincide — and convex (see Sec. 3.3.5). Expansion shocks are the only type of inadmissible discontinuities in HD. Ideal HD and dissipative HD behave completely similarly regarding admissibility of shocks.

In contrast, the MHD equations are non-strictly hyperbolic and non-convex, and have a peculiar type of rotational invariance. Because of these properties, next to expansion shocks also other types of discontinuities can be inadmissible in MHD. The matter is complicated by the

fact that for MHD admissibility of shocks is *different* for the ideal system and the dissipative system. It is said that dissipative MHD does not uniformly approach ideal MHD in the limit of vanishing dissipation.

In ideal MHD several types of intermediate shocks are inadmissible. For this reason intermediate shocks have been considered *extraneous* or *unphysical* since the early sixties [2, 71, 87]. However, recently it has been shown that intermediate shocks are admissible in dissipative MHD [170, 43, 110], and can thus not be termed 'unphysical'.

The MHD system is extremely complex and allows for many types of degeneracies and singularities which can coincide and interact. For these reasons the problem of the admissibility of MHD shocks has probably not been solved yet in full. Much can be learned about the possible pathologies by considering *model problems* of reduced complexity which each retain certain aspects of the singular behavior of the MHD system. In Sec. 9.2 we describe the admissibility of discontinuities in such model systems. Due to space constraints we limit ourselves to sketching the general ideas while omitting technical details which can be found in the literature.

The admissibility of shocks is very different in the planar and the full MHD systems. Planar MHD ($v_z \equiv B_z \equiv 0$) does not allow for Alfvén waves, whereas full MHD does. In Sec. 9.3 we discuss the admissibility of shocks in the planar MHD system. We show how the planar 2D magnetically dominated bow shock flows around cylinders that were discussed in Chap. 6 form excellent illustrations in 2D of the theory on the admissibility of shocks in planar MHD. We compare the performance of various numerical schemes for the calculation of these flows and relate the results to the occurrence of physical and numerical instabilities. In Sec. 9.4 the admissibility of shocks in the full MHD system is discussed. The 3D magnetically dominated bow shock flows around spheres that were discussed in Chap. 7 are shown to be excellent illustrations in 3D of the theory on the admissibility of shocks in full MHD. Intermediate shocks have been found previously in 1D and in some 2D simulation results [12, 147], but the bow shock flows described in Chaps. 6 and 7 are the first clear illustrations in 2D and 3D of the whole variety of intermediate shock phenomena that can arise in MHD flows.

We limit our exposition of the theory of MHD shock admissibility in Secs. 9.3 and 9.4 to sketching general results which are illustrated by analogies with the model systems discussed in Sec. 9.2. A complete and rigorous derivation of the theoretical results is far beyond the scope of this dissertation, not only due to space constraints but also because many aspects of the problem have not been solved yet in full. For instance, theoretical results have only been derived for systems which are limited to variation in one spatial dimension. Some of the reasonings presented in this Chapter have obvious loose ends, and many open prob-

lems remain for which we can only provide speculative answers. We have found the recent literature on this subject very confusing and contradictory [173, 46, 110, 35]. As is often true in such cases, the confusion and contradiction mainly seem to stem from vagueness in concepts, terminology and problem definition. We think that a reasonably consistent picture of the admissibility of shocks in MHD can be distilled from the recent literature. We have found references [103, 102, 48, 46] the most useful. References [170, 173, 110, 35] are also of interest. In this Chapter it is our aim to sketch a consistent theory of the admissibility of MHD shocks, and to verify whether the simulation results with shock fronts of various types that were described in Chaps. 6 and 7 confirm this theory.

9.2 Admissibility of shocks in model systems

9.2.1 Scalar model

Consider the Burgers equation (see also Secs. 3.2.1 and 3.3.5) which describes the evolution of scalar $u(x,t)$ as

$$\frac{\partial u}{\partial t} + \frac{\partial u^2/2}{\partial x} = \eta \frac{\partial^2 u}{\partial x^2}, \tag{9.1}$$

with flux $f(u) = u^2/2$ and the dissipative coefficient η a positive constant. We choose $s = 0$ and $f_{const} = 1/2$ in the Rankine-Hugoniot relation (see Sec. 3.3.1)

$$-su + f(u) = f_{const}. \tag{9.2}$$

Eq. 9.2 then allows for two solutions, $u_1 = 1$ and $u_2 = -1$. Let us consider the case that $\eta \equiv 0$ in Eq. 9.1. In this case Eq. 9.1 allows for discontinuous weak solutions with vanishing shock thickness. The two states satisfying the RH relations can be connected with a shock in two ways, with u_1 either on the left or on the right side of the shock, and with u_2 on the other side.

Fig. 9.1 sketches the behavior of the characteristic curves (see Sec. 3.2.1) with slope $f'(u) = u$ in the xt plane for the two possible configurations. These configurations both are solutions of the integral form of Eq. 9.1 with $\eta \equiv 0$. In Sec. 3.3 we have postulated that only shocks in which the characteristics converge are admissible. Following this criterion, the configuration of Fig. 9.1a is inadmissible, while the configuration of Fig. 9.1b is admissible. We now review several possible shock admissibility criteria and the reasoning which leads to them. We start out with admissibility criteria for discontinuous solutions of the ideal dissipation-free equation ($\eta \equiv 0$ in Eq. 9.1), followed by admissibility criteria for shocks described by the dissipative equation.

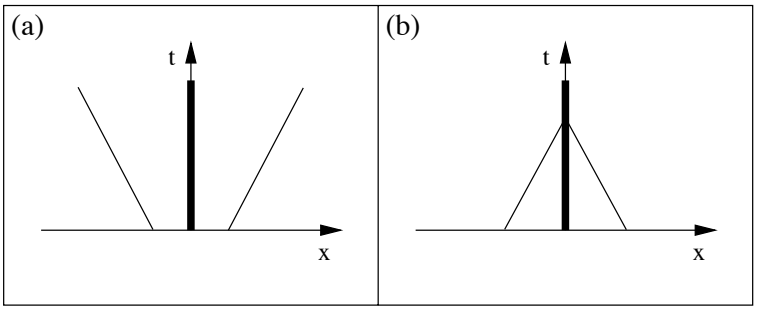

Figure 9.1: *Two possible ways in which a pair of states satisfying the RH relations for the ideal Burgers equation can be connected by a shock (thick). (a) (u_l,u_r)=(-1,1). The characteristics (thin) diverge from the shock on the two sides. This configuration is inadmissible. (b) (u_l,u_r)=(1,-1). The characteristics converge into the shock on the two sides. This configuration is admissible.*

Admissibility of shocks described by the ideal equation

The following are four important criteria used in the literature (e.g. [109]).

- **I1: Steepening criterion**
  The shock of Fig. 9.1b is admissible because it can be formed through wave steepening due to the nonlinearity of the equation (Fig. 3.2), whereas the shock of Fig. 9.1a is inadmissible because it cannot be formed through wave steepening. Indeed, if we replace the discontinuities in Fig. 9.1 by steep linear profiles connecting the left and the right states, then the profile of Fig. 9.1b steepens into a shock because the characteristics are bound to intersect. In contrast, the profile of Fig. 9.1a decays into a rarefaction wave which broadens in time because characteristics diverge.

- **I2: Perturbation criterion**
  Let us perturb the configuration $u(x,t)$ of Fig. 9.1b with a profile $m(x,0)$ which has limited spatial extent such that the weight of the perturbation
  $$M = \int m(x,0)\,dx, \tag{9.3}$$
  is bounded (Fig. 9.2a). The time evolution of the solution of the perturbed problem $u'(x,t) = u(x,t) + m(x,t)$ is governed by the constraint that $\int m(x,t)\,dx$ remains constant in time, as follows from the conservation law Eq. 9.1. Due to the convergence of the

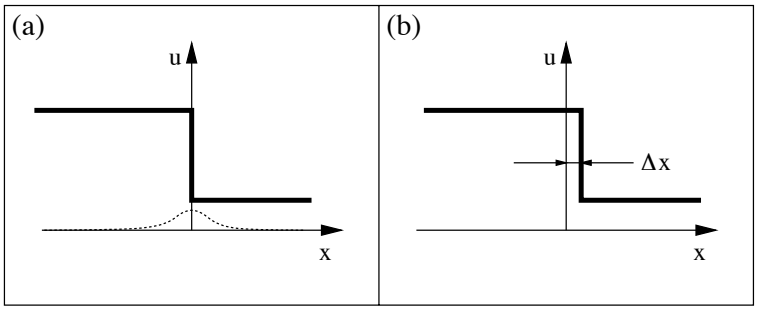

Figure 9.2: *Perturbation of the configuration of Fig. 9.1b with a profile $m(x,0)$ which has limited spatial extent. The solution of the perturbed problem (a) evolves in finite time to the solution represented in (b) with a shock connecting the original left and right state and with the same shock speed (stationary in this case) as the original shock. The shock is translated over a distance Δx.*

characteristics the perturbed system evolves in finite time to the solution of Fig. 9.2b with a shock connecting the original left and right state and with the same shock speed (stationary in this case) as the original shock. The only difference between the unperturbed configuration and the final state of the perturbed problem is that the shock is translated over a distance Δx, with $\Delta x = M/\Delta u$, and $\Delta u = u_l - u_r$. The distance of translation Δx decreases with decreasing perturbation weight M. The evolution of the perturbed system is subject to one constraint, and by adjusting the free parameter of the shock location a solution can be found for which this constraint is satisfied. The shock in the configuration of Fig. 9.1b is stable against perturbations, and is thus admissible. The shock in the configuration of Fig. 9.1a, however, breaks up into a rarefaction wave upon even the smallest perturbation, since characteristics diverge. We say that it is unstable against *generic* perturbations, and thus inadmissible.

- **I3: Lax criterion**
  Motivated by the theory of free boundary value problems [88], the following admissibility criterion has been proposed. The scalar version of the RH relation reads $(f(u_r) - f(u_l))/(u_r - u_l) = s$. This constitutes one equation in three variables. If the values of u_r and u_l are specified externally, then this relation can be satisfied at a discontinuity and determines the shock speed s. Two incoming characteristics specify the values of u_r and u_l, and it is concluded that in this case the shock is admissible. When the characteris-

tics leave the shock, the RH relation is underdetermined and it is concluded that the shock is inadmissible. This criterion is due to Lax [88]. It constitutes a condition on the geometry of shocks and characteristic curves in the xt plane, and is therefore also called the *geometrical* admissibility criterion. Shocks admissible under the Lax criterion are called *Lax shocks*.

- **I4: Linearized stability or evolutionarity criterion**
  The linearized stability or evolutionarity criterion is closely related to the Lax criterion. It is argued that the perturbation problem of the linearized RH relation should have a unique solution for shocks to be admissible [2, 71, 87, 44]. In this case it is said that shocks are *evolutionary* or *linearized stable*. For the scalar case it is found that shocks with impinging characteristics are evolutionary, while shocks with diverging characteristics are non-evolutionary.

In this case of a scalar equation the criteria I1–I4 all give the same result for the admissibility of shocks. These criteria are extended to systems of conservation laws in Sec. 9.2.2. As is shown below, these admissibility criteria for ideal shocks can be related to criteria for dissipative shocks. In the case of physical systems like the HD equations, this allows for instance to relate the ideal criteria I1–I4 to the concept of increasing entropy.

It is interesting to discuss the implications of the obtained results on shock admissibility for the solution of Riemann problems. For the case of the Burgers equation, shocks admissible under criteria I1–I4 allow for a unique solution of all Riemann problems. Riemann problems are well-posed in the usual sense, namely that a unique solution exists and that small changes in the initial conditions (left and right states) only imply small changes in the solution. If this is true, it is said that a continuous solution operator exists for the Riemann problem [46]. For the Burgers equation a continuous solution operator exists which contains the admissible shocks and rarefaction waves [88].

Admissibility of shocks described by the dissipative equation

A co-stationary traveling wave solution of Eq. 9.1 with non-vanishing dissipation satisfies

$$-su + f(u) - f_{const} = \eta \frac{\partial u}{\partial x}. \tag{9.4}$$

We now investigate under which conditions traveling wave solutions with uniform left and right states u_l and u_r connected by a narrow smooth profile are possible. These solutions can be formed through nonlinear steepening and are the analogs of the shocks described by the ideal

equation. The width of the dissipative shock layer is determined by the balance between nonlinear steepening and dissipation. In the uniform regions where $u = u_l$ or $u = u_r$ the dissipative term vanishes, such that the left and the right state still have to satisfy the RH relation Eq. 9.2.

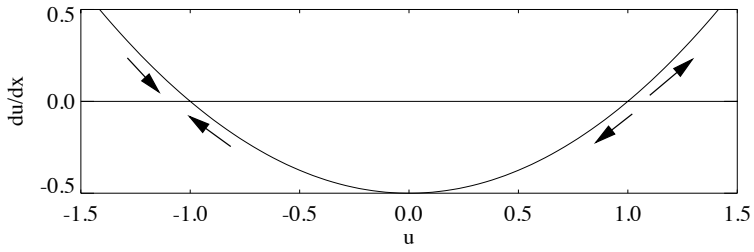

Figure 9.3: *Autonomous system describing viscous profiles of the Burgers equation. The system has fixed points where* $\partial u/\partial x = 0$. $u = 1$ *is an unstable fixed point, but* $u = -1$ *is stable. A viscous profile exists from* $u_l = 1$ *to* $u_r = -1$.

We choose shock speed $s = 0$, flux constant $f_{const} = 1/2$ and dissipation coefficient $\eta = 1$ in Eq. 9.4. The shock structure equation 9.4 now mathematically describes an *autonomous system* of first order, which relates variable u and its derivative $\partial u/\partial x$. This autonomous system can be analyzed using the theory of dynamical systems [113]. This autonomous system has *fixed points* when $\partial u/\partial x = 0$. For the flux function and parameters s and f_{const} under consideration, these fixed points — which satisfy the RH relations — are $u = 1$ and $u = -1$. Fig. 9.3 plots the relation between u and $\partial u/\partial x$. The fixed points are located where this curve crosses the $\partial u/\partial x = 0$ axis, and we want to determine now if a trajectory or a *viscous profile* exists on the plotted curve which can connect the two fixed points. Strictly speaking we should rather call the profile a *dissipative profile*, but the terminology of the Navier-Stokes case for which viscosity acts as dissipation is often used in a generalized manner.

Suppose $u_l = 1$ and $u_r = -1$. Can these two states in this ordering be connected by a viscous profile? If we start from $u_l = 1$ and want to decrease u_l towards $u_r = -1$ in moving to the right (increasing x), we see from the curve in Fig. 9.3 that $\partial u/\partial x$ becomes negative, such that u can indeed decrease further while moving further to the right (increasing x). When we approach $u_r = -1$, $\partial u/\partial x$ increases towards zero. We can reach $u_r = -1$, but once we reach this right state, $\partial u/\partial x = 0$, and

u does not change anymore. This is exactly what we want: $u_l = 1$ can be connected to $u_r = -1$ by a viscous profile. For given left and right states this viscous profile is unique, and an explicit solution can be found [90]. If we would take $u_l = -1$ and $u_r = 1$, then we see that no viscous profile exists, because state $u = -1$ cannot be increased in going to the right. Fixed point $u = 1$ is an *unstable node*, because the slope of the curve is positive, and fixed point $u = -1$ is a *stable node*, with negative slope. In going from left to right (increasing x), we can connect an unstable node with a stable node via a viscous profile. For the dissipative equation, admissible shocks are shocks which have a viscous profile. The configuration of Fig. 9.1a, with diverging characteristics, is not admissible, while the configuration of Fig. 9.1b, with converging characteristics, is admissible.

As in Fig. 9.2 localized perturbation of the viscous shock by a perturbation $m(x,t)$ with finite weight M results in a translation of the shock over a distance Δx which is determined by the constraint that $\int m(x,t)\,dx$ remains constant in time. The translated shock has the same left and right states, shock speed and shock profile as the original shock. The existence of the viscous profile and the behavior under perturbations does not depend on the magnitude of the dissipation η, so we say that the shock profile is *uniformly stable* in the dissipative parameter.

An additional requirement for the admissibility of the shock is that the autonomous system has to be *structurally stable*, which means that small variations in shock speed s, flux constant f_{const} and dissipative coefficient η (which imply small variations in the fixed points) may not change the existence and stability properties of viscous profiles. It is intuitively clear that in the above described case the autonomous system is structurally stable, and this can be proven rigorously as well [48].

Ideal solutions as uniform vanishing viscosity limits of dissipative solutions

An important observation is that precisely the shocks which are admissible in the ideal analysis (Lax shocks) turn out to have viscous profiles! The (ideal) Lax criterion and the (dissipative) viscosity admissibility criterion give the same result for the admissibility of shocks in the respective ideal and dissipative context. This suggests that solutions of the ideal equation 9.1 with $\eta \equiv 0$ may be the *vanishing viscosity limits* of solutions of the dissipative equation 9.1. The admissibility properties of dissipative shocks are indeed uniform in the dissipative parameter, which is required if one wants to take the limit of *vanishing viscosity* in a meaningful way. It can be proven rigorously [48, 90] that in the limit of vanishing viscosity the solutions of the dissipative equation 9.1

uniformly approach the solutions of the ideal equation ($\eta \equiv 0$). It would seem that this behavior should always arise, but in the following Sections we show that this is not the case.

The fact that the ideal and dissipative physical systems uniformly approach each other warrants the use of the *dissipative* viscosity admissibility criterion to determine or motivate the admissibility of shocks in the *ideal* system, and vice versa. This means that the ideal criteria I1–I4 can be justified *a posteriori* by the results of the viscosity admissibility study.

9.2.2 Convex strictly hyperbolic system

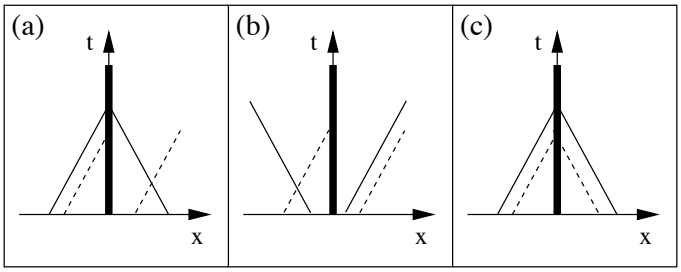

Figure 9.4: *Shock configurations for a* 2×2 *system. (a) Lax shock with* $n+1$ *converging characteristics. (b) Undercompressive shock with less than* $n+1$ *converging characteristics. (c) Overcompressive shock with more than* $n+1$ *converging characteristics.*

Most of the results on shock admissibility described above for the Burgers equation carry over to the case of a convex strictly hyperbolic system of conservation laws. In this Section we do therefore not repeat all considerations, but we limit the discussion to some aspects which are slightly different from the scalar case.

Consider the 2×2 *system* of strictly hyperbolic conservation laws

$$\frac{\partial}{\partial t}\begin{bmatrix} u \\ v \end{bmatrix} + \frac{\partial}{\partial x}\begin{bmatrix} f(u,v) \\ g(u,v) \end{bmatrix} = 0, \tag{9.5}$$

with the flux functions f and g chosen such that wave speeds cannot coincide. In the xt plane 2 families of characteristic curves exist. Fig. 9.4 shows some possible shock configurations that can arise for a 2×2 system. For the configuration in Fig. 9.4a exactly one family of characteristics converges into the shock, while the other family has one diverging and one converging characteristic. This type of shock is called a Lax shock. For a general strictly hyperbolic $n \times n$ system a Lax shock has $n+$

1 converging characteristics. It is explained below that for a strictly hyperbolic system all admissible shocks have to be of this type. The shock in Fig. 9.4b has less than $n+1$ converging characteristics, and is called *undercompressive*. The shock in Fig. 9.4c is called *overcompressive* since it has more than $n+1$ converging characteristics.

Admissibility of shocks described by the ideal system

Some of the ideal admissibility criteria I1–I4 that were described above have to be altered slightly to make them applicable to systems of conservation laws.

- **I2: Perturbation criterion**

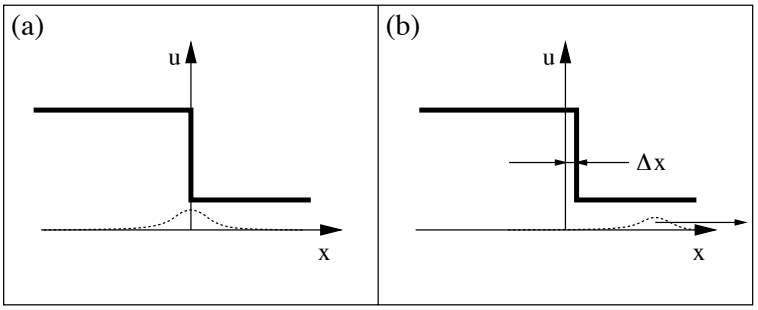

Figure 9.5: *Perturbation of the configuration of Fig. 9.4a with a profile which has limited spatial extent (only the u component is sketched). The solution of the perturbed problem (a) evolves in finite time to the solution represented in (b) with a shock which connects the original left and right state and which has the same shock speed (stationary in this case) as the original shock, and with a wave perturbation which travels away from the shock. The shock is translated over a distance Δx.*

Let us perturb the u and v components of the configuration of Fig. 9.4a with perturbation profiles $m_u(x,0)$ and $m_v(x,0)$ which have bounded weight (Fig. 9.5a). The time evolution of the solution of the perturbed problem is now governed by the two constraints that $\int m_u(x,t)\,dx$ and $\int m_v(x,t)\,dx$ remain constant in time, as follows from the conservation laws. The perturbed system evolves in finite time to the solution of Fig. 9.5b with a shock which connects the original left and right state and which has the same shock speed (stationary in this case) as the original shock, and with a wave perturbation traveling away from the shock. The wave can travel

outwards because one of the characteristics diverges away from the shock (Fig. 9.4a). The shock is translated over a distance Δx which is determined by the weights of the perturbation. The distance of translation Δx decreases with decreasing perturbation weight. The evolution of the perturbed system is subject to two constraints, which can be satisfied by adjusting the shock location (one free parameter) and by sending out a wave. The shock in the configuration of Fig. 9.4a is stable against perturbations, and is thus admissible. The shock in the configuration of Fig. 9.4b, however, breaks up into a rarefaction wave upon even the smallest perturbation. It is unstable against *generic* perturbations, and thus inadmissible.

- **I3: Lax criterion**
  For a general $n \times n$ system, the RH relations constitute n relations between $2n+1$ variables. $n+1$ variables have thus to be specified externally, which means that $n+1$ characteristics have to impinge on a shock in order to make the shock admissible. Shocks with $n+1$ impinging characteristics are called Lax shocks. Lax shocks are admissible, and overcompressive and undercompressive shocks are inadmissible.

- **I4: Linearized stability or evolutionarity criterion**
  For a general $n \times n$ system, the perturbation problem of the linearized RH relations has a unique solution when $n+1$ characteristics impinge on the shock. It is concluded that only shocks with $n+1$ impinging characteristics are admissible. Those shocks are called evolutionary.

Admissibility of shocks described by the dissipative system

For given left and right states, dissipative shocks are admissible when traveling wave solutions exist which connect the two states. The shock structure equations — the systems version of Eq. 9.4 — now mathematically describe a higher order autonomous system, which relates state variables and their spatial derivatives. This autonomous system can be analyzed using the theory of dynamical systems [113]. The fixed points of the autonomous system satisfy the RH relations. For a convex strictly hyperbolic system, two fixed points generally exist for given shock speed and flux constants in Eq. 3.73. One fixed point is an unstable node, and the other one is of saddle type. There thus exists a unique viscous profile connecting the two fixed points. This profile is structurally stable. Configurations like in Fig. 9.4b do not have a viscous profile and are not admissible, while configurations like in Fig. 9.4a do have a viscous profile and are admissible.

As in Fig. 9.5 localized perturbation of the viscous shock results in a translation of the shock over a distance Δx and in the emission of a wave. The translated shock has the same left and right states, shock speed and shock profile as the original shock. The existence of the viscous profile and the behavior under perturbations does not depend on the magnitude of the dissipative coefficients, so we say that the shock profile is *uniformly stable* in the dissipative parameters.

9.2.3 Non-strictly hyperbolic system

Consider the non-strictly hyperbolic system

$$\frac{\partial}{\partial t}\begin{bmatrix} u \\ v \end{bmatrix} + \frac{\partial}{\partial x}\begin{bmatrix} a\,u^2/2 + b\,v \\ v^2/2 \end{bmatrix} = 0, \tag{9.6}$$

with a and b positive constants. We follow the analysis of this model problem which was presented in [103]. The characteristic speeds are $\lambda_1 = a\,u$ and $\lambda_2 = v$. They coincide when $au = v$. The system is thus non-strictly hyperbolic.

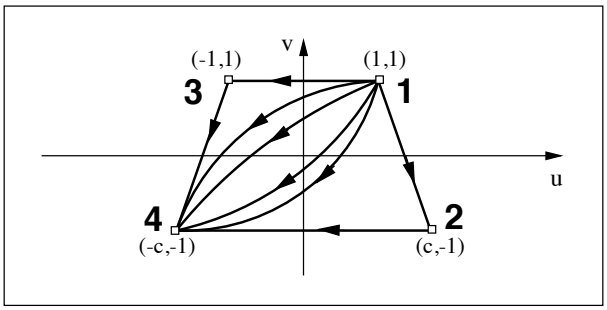

Figure 9.6: *Points in phase space uv that can be connected to the state* $(1,1)$ *by a discontinuity with speed zero. The constant* $c = \sqrt{1+4b/a}$. *The thick curves with arrows represent viscous profiles.*

In Fig. 9.6 we show which points in phase space uv can be connected to the state $(1,1)$ by a discontinuity with speed zero. The state $(1,1)$ and the shock speed determine the flux constants in Eq. 3.73, and this equation then has the four solutions indicated in Fig. 9.6. We now investigate the admissibility of ideal and dissipative shocks.

Admissibility of shocks described by the ideal system

A simple calculation of the characteristic speeds in states 1, 2, 3 and 4 of Fig. 9.6 shows that according to the Lax and evolutionarity criteria

(I3 and I4), shocks 1–2, 1–3, 2–4 and 3–4 are admissible because they have $n + 1 = 3$ converging characteristics. Shock 1–4, however, has 4 incoming characteristics, and is thus overcompressive and inadmissible! Shocks 2–3 and 3–2 are undercompressive.

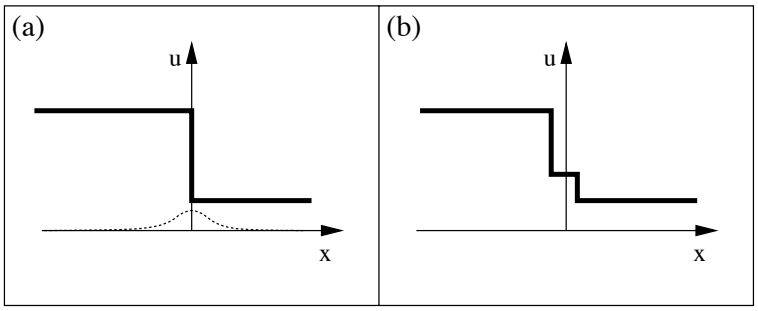

Figure 9.7: *A localized perturbation of an ideal 1–4 overcompressive shock makes the shock split into two shocks of 1–3 and 3–4 (or 1–2 and 2–4) types with the same speed.*

1–4 shocks are indeed unstable against generic perturbations (criterion I2). Fig. 9.7 sketches how a localized perturbation of a 1–4 overcompressive shock makes the shock split into two shocks of 1–3 and 3–4 (or 1–2 and 2–4) types. The time evolution of the solution of the perturbed problem is again governed by the two conservation constraints that $\int m_u(x,t)\,dx$ and $\int m_v(x,t)\,dx$ remain constant in time. In the case of an overcompressive shock, a wave cannot be sent out from the shock because all the characteristics converge into the shock! The two constraints can also not be satisfied by adjusting the free parameter which describes the shock location, because this is only one free parameter. It follows from detailed analysis of the time evolution [103] or from numerical simulation that the shock necessarily has to break up. The two shocks still connect the original left state with the original right state, and have the same speed as the original overcompressive 1–4 shock. The distance of separation between the two shocks decreases with decreasing perturbation weight.

Like the non-evolutionary undercompressive shock of Fig. 9.1a, 1–4 shocks are inadmissible according to the evolutionarity criterion, but the behavior of these two types of shocks upon perturbation is quite different. The shock of Fig. 9.1a degenerates completely upon the smallest perturbation and the resulting flow is not in any way close to the unperturbed flow for large times. The 1–4 shock also ceases to exist upon a generic perturbation, but the flow after perturbation remains close to the unperturbed flow for all times. In some flow problems 1–2 and 2–4

(and also 1–3 and 3–4) shocks coincide and may then be considered as a single 1–4 shock. In this sense 1–4 shocks are admissible in ideal flows described by system 9.6.

Admissibility of shocks described by the dissipative system

State 1 in Fig. 9.6 is an unstable node, 4 is a stable node, and 2 and 3 are saddles. Shocks 1–2, 1–3, 2–4 and 3–4 have unique viscous profiles and are thus admissible. Shock 1–4 has a one-parameter family of viscous profiles, and is thus admissible too.

Localized perturbation of a viscous 1–4 shock does *not* result in break-up of the shock in two separate shocks! Again, translation of the shock can only account for one constraint, and the other constraint cannot be satisfied by sending out a wave because the shock is overcompressive. However, the one-parameter family of viscous profiles provides another free parameter. Upon perturbation, the shock is translated and the viscous profile jumps to a different member of the one-parameter family, such that the two constraints are met. 1–4 shocks are thus admissible solutions of the dissipative system. The existence of the viscous profile and the behavior under perturbations do not depend on the magnitude of the dissipative coefficients, so we say that the shock profile is *uniformly stable* in the dissipative parameters. There seems to be a contradiction between the fact that 1–4 shocks are non-evolutionary in the ideal system, but have viscous profiles in the dissipative system. This contradiction is partially resolved by noting that 1–4 shocks can arise in ideal flows as the limit of coinciding 1–2 and 2–4 (or 1–3 and 3–4) shocks.

9.2.4 Rotationally invariant non-strictly hyperbolic system

Consider the non-strictly hyperbolic system

$$\frac{\partial}{\partial t}\begin{bmatrix} u \\ v \end{bmatrix} + \frac{\partial}{\partial x}\begin{bmatrix} u\,(u^2+v^2) \\ v\,(u^2+v^2) \end{bmatrix} = 0. \tag{9.7}$$

We follow the analysis of this model problem which was presented in [102] and [48]. The characteristic speeds are $\lambda_1 = u^2+v^2$ and $\lambda_2 = 3\,(u^2+v^2)$, which describe waves in the angular and radial directions in phase space respectively (see Fig. 9.10). The characteristic speeds coincide when $u = v = 0$. The system is thus non-strictly hyperbolic. We can consider the restricted system obtained by setting $v \equiv 0$. This restricted system has the non-convex flux function $f(u) = u^3$ which is of the type discussed in Sec. 3.3.5. The flux function $\mathbf{F}$ of system 9.7 satisfies a peculiar kind of *rotational invariance* [48], namely that

$$\mathbf{F}(\mathbf{U}) = \phi(||\mathbf{U}||^2)\,\mathbf{U}, \tag{9.8}$$

with ϕ the identity function in this case.

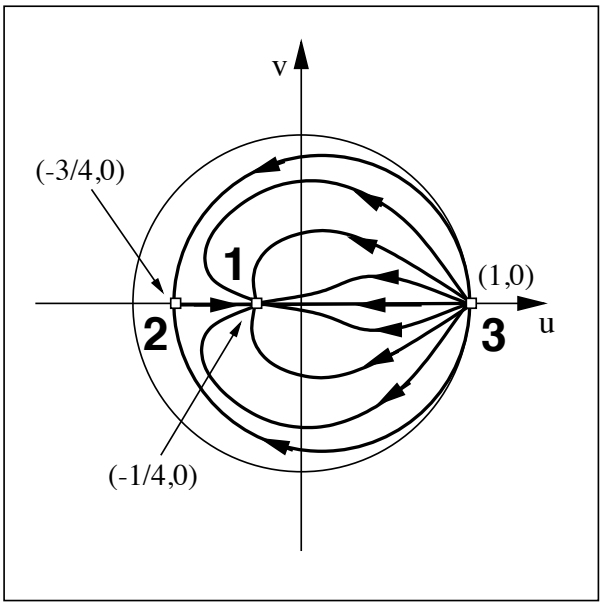

Figure 9.8: *Points in phase space uv that can be connected to the state* $(1,0)$ *by a discontinuity with speed 13/16. The thick curves with arrows represent viscous profiles.*

In Fig. 9.8 we show which points in phase space uv can be connected to the state $(1,0)$ by a discontinuity with speed $13/16$. The state $(1,0)$ and the shock speed determine the flux constants in Eq. 3.73, and this equation then has the three solutions indicated in Fig. 9.8. We now investigate the admissibility of ideal and dissipative shocks.

Admissibility of shocks described by the ideal system

A simple calculation of the characteristic speeds in states 1, 2 and 3 of Fig. 9.8 shows that shock 3–1 is overcompressive (and 1–3 thus undercompressive), 3–2 is a Lax shock and 2–1 is Lax too. According to the Lax and evolutionarity criteria (I3 and I4), shocks 3–2 and 2–1 are admissible because they have $n+1=3$ converging characteristics. Shock 3–1 has 4 incoming characteristics and is thus inadmissible!

3–1 shocks are indeed unstable against generic perturbations (criterion I2). Fig. 9.9 sketches how a localized perturbation of a 3–1 overcompressive shock makes the shock split into two shocks. This can be understood by a reasoning on conservative constraints and converging

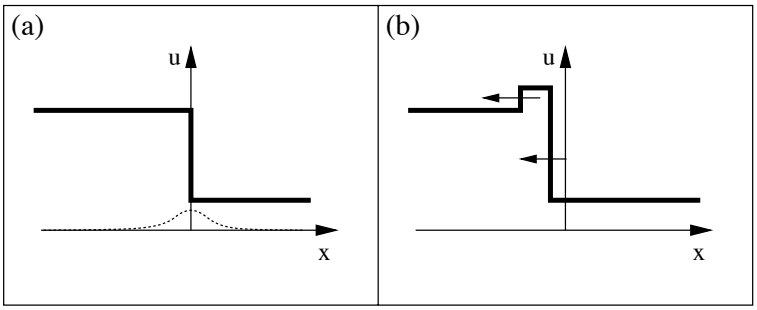

Figure 9.9: *A localized perturbation of an ideal 3–1 overcompressive shock makes the shock split into two shocks which propagate away from the location of the original shock.*

characteristics similar to the reasoning presented in Sec. 9.2.3. A crucial difference with the case of Sec. 9.2.3, however, is that the two shocks do *not* propagate with the same speed as the original unperturbed shock. This behavior, like most other peculiar properties of system 9.7 described in this Section, is generic for non-strictly hyperbolic systems with a rotationally invariant flux function [48]. The distance of separation between the two shocks thus increases in time without bounds for even the smallest perturbation.

The 3–1 shock described by system 9.7 thus behaves similarly to the non-evolutionary undercompressive shock of Fig. 9.1a, in the sense that the resulting flow is not in any way close to the unperturbed flow for large times. 3–1 shocks are thus inadmissible in ideal flows, not only according to the evolutionarity criterion, but also according to the perturbation criterion. 3–1 shocks cannot exist in ideal flows. This behavior is very different from the behavior of the 1–4 shocks in the system of Sec. 9.2.3.

Remark that in the restricted system 9.7 with $v \equiv 0$ ideal shock admissibility is entirely different. The rotational mode λ_1 disappears. 3–1 shocks become admissible Lax shocks. 2–1 shocks remain Lax shocks, but 3–2 and 2–3 shocks are both undercompressive (Fig. 3.17). The presence of the rotational wave mode in the full system thus completely destabilizes ideal 3–1 shocks, and stabilizes 3–2 shocks.

Admissibility of shocks described by the dissipative system

In Fig. 9.8 state 1 is a stable node, 3 is an unstable node, and 2 is a saddle. Shocks 3–2 and 2–1 have unique viscous profiles and are thus admissible. Shock 3–1 has a one-parameter family of viscous profiles, and is thus admissible too.

Localized perturbation of a viscous 3–1 shock does *not* result in break-up of the shock in two separate shocks when the perturbation weight is small. Upon perturbation, the shock is translated and the viscous profile jumps to a different member of the one-parameter family, such that the two conservation constraints are met. 3–1 shocks are thus admissible solutions of the system 9.7 with dissipation. This conclusion seems to be analogous to the conclusion for the 1–4 shocks described by system 9.6 as discussed in Sec. 9.2.3.

However, there are two crucial differences.

First, when the weight M_v of the perturbation of v increases, the viscous profile of the 3–1 shock approaches the 3–2–1 orbit (Fig. 9.8). When M_v is further increased, the 3–1 shock splits up into a 3–2 and a 2–1 shock. Those shocks propagate away with speeds which are different from the speed of the original unperturbed shock (Because of the larger M_v state 2 shifts to the left in Fig. 9.8!). The resulting flow is not in any way close to the unperturbed flow for large times, similar to the ideal case discussed above.

Second, the critical perturbation mass M_v required for break-up of the shock decreases with decreasing dissipation, and vanishes for vanishing dissipation. This means that 3–1 shocks become less stable when the dissipation is decreased. For the 3–1 shock the behavior under perturbations does thus depend on the magnitude of the dissipative coefficients, so we conclude that the shock profile is *not* uniformly stable in the dissipative parameters!

3–1 shocks are admissible in the dissipative system, and inadmissible in the ideal system. This contradiction is resolved by the fact that the dissipative 3–1 shocks become generically unstable for vanishing dissipation. The dissipative system thus approaches the ideal system for vanishing dissipation, but not in a uniform way, since 3–1 shocks are admissible in the dissipative system and not in the ideal system.

Solution of Riemann problems

It is interesting to investigate the implications of the above described results on shock admissibility for the solution of Riemann problems. In Fig. 9.10 a Riemann problem with $\mathbf{U}_l = (1,0)$ and $\mathbf{U}_r = (-1,0)$ is sketched in phase space. Two different solutions are proposed.

The restriction of the system to the u-axis suggests the solution which contains a sonic shock connecting $\mathbf{U}_l$ with $\mathbf{U}^* = (-1/2,0)$, followed by a rarefaction wave which connects $\mathbf{U}^*$ with $\mathbf{U}_r$. This is the compound shock type solution which has been discussed in Sec. 3.3.5 for a non-convex scalar system. Another solution is a single rotational wave (associated with the angular mode λ_1) which brings $\mathbf{U}_l$ directly to $\mathbf{U}_r$.

Which solution is valid? The reader may anticipate from the above

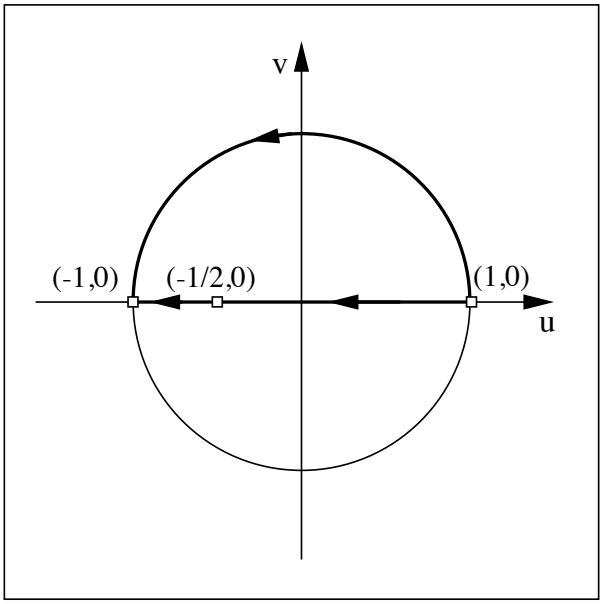

Figure 9.10: *Riemann problem with* $\mathbf{U}_l = (1,0)$ *and* $\mathbf{U}_r = (-1,0)$. *Two different solutions are proposed (thick lines with arrows).*

discussion that the answer depends on whether one considers the ideal or the dissipative system.

In the ideal system, the compound shock solution cannot arise because the sonic shock is a 3–1 shock which is inadmissible in the ideal system. The 3–2 rotational shock is admissible, so the solution to the Riemann problem is the rotational shock. The Riemann problem is thus well-posed, because the solution is unique and depends continuously on the initial data. Indeed, consider a Riemann problem with left state $\mathbf{U}_l = (1,0)$ and right state $\mathbf{U}_r = (-\cos\delta, \sin\delta)$. The solution with a rotational wave over angle $\pi - \delta$ for non-vanishing δ goes over smoothly in the solution with angle π for vanishing δ.

It is remarkable that the solution of the Riemann problem for the ideal system restricted to the u-axis — with the compound shock — is very different from the Riemann problem solution for the full system. How can a Riemann problem which is in a way 'the same' in the two cases have so different solutions? The answer lies in the influence of the rotational mode, which is present in the full system but not in the restricted system. On one hand the rotational mode destabilizes ideal 3–1 shocks such that compound shocks cannot arise in Riemann problem

solutions of the full system. On the other hand the rotational mode introduces a new wave mode which can play the role of the 3–1 shock — which consists in changing the sign of u — in solutions of Riemann problems for the full system.

In the dissipative system, the compound shock solution can arise because the 3–1 shock is admissible. The 3–2 rotational shock is admissible too, but due to the symmetry of the initial condition — $v \equiv 0$ in the initial condition of the Riemann problem, and thus has to remain zero in the Riemann problem solution, also in the profile of the viscous shock —, the compound shock solution is obtained. This symmetry constraint did not play in the ideal problem because the 3–2 rotational shock has no profile in the ideal case!

The fact that Riemann problems can have a completely different solution in the ideal and dissipative system has been illustrated beautifully by Freistuehler and Pitman [48]. They perform numerical simulations of the ideal problem using a dissipation-free numerical technique based on the *Glimm scheme*, and do indeed find the solution with the rotational wave for the Riemann problem of Fig. 9.10. Use of numerical techniques with intrinsic numerical dissipation results in the solution with the compound shock, because the numerical dissipation plays a role analogous to a physical dissipation.

Freistuehler and Pitman [48] also analyze numerically the *vanishing viscosity limit* solution of the Riemann problem of Fig. 9.10. It turns out that in the limit of vanishing viscosity the solution of the Riemann problem of Fig. 9.10 is the compound shock solution! How can the vanishing viscosity limit solution be different from the solution of the ideal problem? The reason for this is that the dissipative system does not uniformly approach the ideal system for vanishing dissipation. We propose the following analogy to illustrate this.

Let us first recall the concept of a uniformly convergent row of functions. The row of functions $\{y_n(x) = exp(-n\,x) | x \in (0, +\infty), n = 0, 1, 2, ...\}$ clearly converges to the function $y(x) = 0$ in $(0, +\infty)$, but it is said that the convergence is not uniform because if one wants to approach the limit $y(x) = 0$ within a certain distance ϵ, then arbitrary large values of n are required if one moves closer to $x = 0$ (Fig. 9.11, left panel). The limit function $y(x) = 0$ can be extended continuously to the domain $x \in [0, +\infty)$ which includes the point $x = 0$ by defining $y(0) = 0$.

In [48] the Riemann problem with left state $\mathbf{U}_l = (1, 0)$ and right state $\mathbf{U}_r = (-\cos\delta, \sin\delta)$ is investigated numerically for the two limits of vanishing dissipation and vanishing δ. For a finite value of the dissipation and δ, it is found that the solution to the Riemann problem consists of some kind of 'mixed solution' with elements from both the rotational wave and the compound shock. For a constant δ and decreasing dissipa-

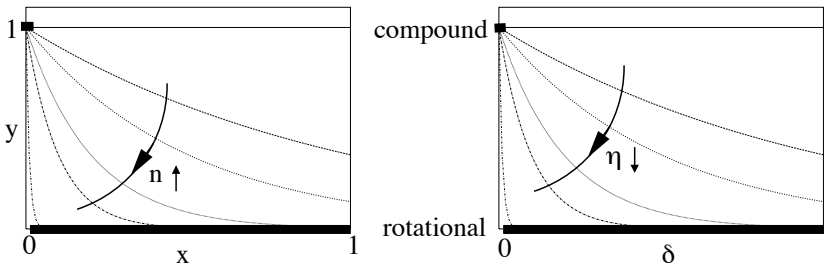

Figure 9.11: *Left panel: The row of functions* $\{y_n(x) = exp(-n\,x) | x \in (0, +\infty), n = 0, 1, 2, ...\}$ *clearly converges to the function* $y(x) = 0$ *in* $(0, +\infty)$ *(thick), but the convergence is not uniform. Right panel: The vanishing viscosity approach for Riemann problems does not converge uniformly.*

tion, the solution becomes more like a rotational wave, and the rotational solution is perfectly obtained in the limit of vanishing dissipation. For constant dissipation but decreasing δ, the solution becomes more like the compound shock solution, and the compound shock solution is perfectly obtained in the limit of $\delta = 0$. The vanishing viscosity limits of the Riemann problem solutions — $\eta \downarrow 0$ with δ constant — do thus not contain compound shocks, except for the case $\delta = 0$, for which a compound shock solution is obtained. Remark that for vanishing dissipation the compound shock solution becomes generically unstable because the perturbation weight required for destruction of the 3–1 shock vanishes [46]. The vanishing viscosity limit of the Riemann problem is not uniform, or the vanishing viscosity approach — consisting in determining the vanishing viscosity limit of flow solutions — does not converge uniformly for the system 9.7. The vanishing viscosity Riemann solution operator is not continuous. The right panel of Fig. 9.11 draws an analogy between this behavior and the non-uniformly converging row of functions described above.

The non-uniform convergence of the vanishing viscosity approach for the Riemann problems described above is related to the fact that 3–1 shocks are stable non-uniformly in the dissipation strength. Indeed, 3–1 shocks are less stable for smaller dissipation, and become less dominant in Riemann problem solutions for a given δ when the dissipation is decreased. Both these phenomena are manifestations of the fact that the dissipative system does not uniformly approach the ideal system for vanishing dissipation [46].

For the ideal system the Riemann problem solution for $\delta = 0$ contains the rotational wave — like for non-vanishing δ. The ideal Riemann

solution operator is thus continuous, and can be interpreted as the continuous extension of the vanishing viscosity Riemann solution operator.

9.2.5 Discussion

The most important lessons to be learned from the discussion in this Section are that for non-strictly hyperbolic systems shock admissibility can be very different in the ideal and the dissipative case, and that a dissipative system may not uniformly approach its associated ideal system for vanishing dissipation.

The criterion of evolutionarity is not a good criterion for shock admissibility in dissipative systems because non-evolutionary shocks can be admissible in dissipative systems. Even in the ideal context the evolutionarity criterion is not very appropriate to determine shock admissibility, because it does not differentiate enough. For instance, the overcompressive shock of Fig. 9.4c is considered inadmissible according to the evolutionary criterion, but the behavior of this type of shock under perturbations is very different for different non-strictly hyperbolic systems. The overcompressive 3–1 shock discussed in Sec. 9.2.4 is inadmissible under the perturbation criterion, but the 1–4 shock discussed in Sec. 9.2.3, although non-evolutionary, can arise in ideal flows as the limit of two coinciding admissible shocks. Evolutionarity is thus not a good criterion to determine shock admissibility. Most authors agree with this conclusion [173, 109], but other authors do not agree [107, 35].

Freistuehler and Pitman [48] discuss how for some non-strictly hyperbolic systems the non-uniform nature of the vanishing dissipation limit has profound implications for the numerical calculation of solutions. A clear distinction has to be made between solving the ideal system and its associated dissipative system. For some problems the ideal and the dissipative solutions are entirely different. Numerical solutions of the ideal system are to be calculated by numerical methods which do not introduce any numerical dissipation. Solutions of the dissipative system are obtained when numerical methods are used which introduce numerical dissipation. Stability of shocks may depend on the precise mechanism and magnitude of the dissipation, such that the dissipative terms should preferably be discretized explicitly. When the dissipation is decreased there is no guarantee that the ideal solution is approached, as the vanishing viscosity limit may differ from the ideal solution.

The HD system is strictly hyperbolic. The associated dissipative system — the Navier-Stokes equations — approaches the ideal system — the Euler equations — uniformly for vanishing dissipation. Ideal HD is thus a good approximation of dissipative HD with small dissipation. We have to remark that this holds at least as far as shock admissibility and Riemann problem solutions are concerned, while it may not hold

in the context of turbulence. Dissipative shock admissibility criteria can be applied directly to select admissible shock solutions of the ideal system. This is called the entropy or vanishing viscosity approach to determine the admissibility of ideal shocks. Numerical simulations with codes which introduce numerical dissipation produce solutions which approach solutions of the ideal system when the (numerical) dissipation is decreased.

In contrast, the MHD system is non-strictly hyperbolic and many of the desirable properties that were sketched above for the HD system do not hold. This is discussed in more detail in the following sections.

9.3 Planar MHD

9.3.1 Admissibility of shocks in planar MHD

The 6×6 system of planar MHD (Eq. 3.12 with $v_z \equiv B_z \equiv 0$) in one dimension has six characteristic waves: two fast waves which propagate with speeds $v_x \pm c_{fx}$, two slow waves with propagation speeds $v_x \pm c_{sx}$, and entropy and divergence waves which propagate with speed v_x (Eq. 3.35). The planar MHD system is non-strictly hyperbolic, because in the direction perpendicular to the magnetic field the slow wave speed c_{sx} vanishes, such that the slow characteristic speeds $v_x \pm c_{sx}$ coincide with the speed v_x of the entropy and divergence waves. The Alfvén waves, which are rotational waves of the type discussed in Sec. 9.2.4, are not present in planar MHD. The planar MHD system is not rotationally invariant.

Shock admissibility in the planar MHD system is analogous to the case of the non-rotationally invariant and non-strictly hyperbolic system discussed in Sec. 9.2.3. In addition the fast and slow characteristic fields are non-convex, such that compound shocks can occur (see Sec. 3.3.5). The discussion in Sec. 3.3 showed that for given shock speed s and flux constant vector $\mathbf{F}_{const}$ the RH relation 3.73 has up to four solutions which can be connected by shocks. Fig. 3.9b shows an example. The four states are labeled 1, 2, 3 and 4 in order of increasing entropy (Fig. 3.7).

Let us first consider the ideal system. Shocks which do not increase the entropy are undercompressive and thus non-evolutionary. Shocks 1–2, 1–3, 2–4 and 3–4 are evolutionary and are thus admissible. This means that 1–3 and 2–4 intermediate shocks are admissible in planar ideal MHD. The 1–4 shock is overcompressive, and the 2–3 shock is undercompressive. According to the evolutionarity criterion they thus both are inadmissible. However, analogous to the case of the 1–4 shock in Sec. 9.2.3, the 1–4 shock can arise in ideal MHD flows when 1–2 and 2–4 (or 1–3 and 3–4) shocks coincide.

For the dissipative system, the 1–2, 1–3, 2–4 and 3–4 shocks have a unique viscous profile. The 1–4 shock has a 1-parameter family of viscous profiles. Because of the non-convexity of the flux function, compound shocks arise. The 2–3 shock does not have a viscous profile. When the flow is such that a 2–3 shock would be required, a compound shock with a 1=2–3 or 2–3=4 sonic shock preceded or followed by a rarefaction wave is obtained instead [109].

Myong and Roe [109, 110] show that with these admissible waves all planar MHD Riemann problems have a unique solution. The planar Riemann problem is thus well-posed.

The admissibility of shocks is thus similar in the ideal and the dissipative cases. The only problem seems to be the 1–4 shock which has a viscous profile which is stable uniformly in the dissipation, but which is not evolutionary. However, this contradiction can partially be resolved by realizing that the 1–4 shock can be found in ideal flows when 1–2 and 2–4 (or 1–3 and 3–4) shocks coincide, and that small perturbations split up the 1–4 shock over a distance which vanishes for vanishing perturbation weight. This indicates that the dissipative system uniformly approaches the ideal system for vanishing dissipation. It can thus be speculated that the vanishing viscosity limit of dissipative flow problems converges to the ideal solution. This would mean that in numerical simulations the ideal solution can be approached by refining the grid and thus reducing the numerical dissipation. Myong (private communication) indeed argues that the solution of the planar MHD Riemann problem which was proposed in [109, 110] is valid for the ideal system as well as for the dissipative system.

9.3.2 Shock types in 2D magnetically dominated bow shock flows

All shocks of type 1–2, 1–3, 2–4, 3–4 and 1–4 are admissible in planar MHD. Compound shocks with 1=2–3 and 2–3=4 intermediate shocks can arise in flow problems. Fast 1–2 and slow 3–4 shocks have of course been known for a long time. All the other types of shocks have been found recently in 1D numerical simulation results [12, 172], and the presence of 1–3 and 1–4 shocks has been claimed in simulated time-dependent 2D flows [146]. The planar magnetically dominated bow shock flows around cylinders that were discussed in Chap. 6 are the first clear example of 2D flows containing intermediate shocks. Moreover, these flows contain *all* the shock types allowed in planar MHD flows, and form thus excellent new illustrations in 2D of the theory on the admissibility of shocks in planar MHD.

We recall from Figs. 6.7, 6.9 and 6.10 that shock segments A–B and D–E are of 1–2 type, B–D is 1–3, E–F is 1–4, D–G–H–I is 2–4, 2=3–4

or 3–4 depending on the exact location along the shock front, and E–H is a tangential discontinuity. Shock segment E–G is a 1=2–3=4 double compound shock. This type of shock is required for the solution of some planar MHD Riemann problems [110], and it is remarkable that the shock E–G forms a double steady xy compound shock which is mathematically completely equivalent to the double time-dependent xt compound shock that was described in [110]. This has been discussed in detail in Sec. 6.4.3.

Falle and Komissarov [35] argue that the 1–4 shock front in the magnetically dominated bow shock flows breaks up at points D and E (Fig. 6.9) because the 1–4 shock is non-evolutionary. We argue that the 1–4 front does not break up because of evolutionarity reasons, but because the intermediate 1–4 shock cannot exist for angles between the upstream magnetic field and the shock normal which are larger than a critical angle. This critical angle is 3° (Fig. 3.9c) for the flow of Fig. 6.9. The break-up of the 1–4 shock front has thus nothing to do with non-evolutionarity or instability against generic perturbations, but is due to the properties of the RH relations.

The planar magnetically dominated bow shock flows described in Chap. 6 were obtained by simulation with a numerical scheme which introduces numerical dissipation. Based on the discussion on vanishing viscosity limits given above, we argue that the solution we obtain approaches the solution to the ideal problem and that the ideal solution thus most probably has the topology of Fig. 6.7.

9.3.3 Numerical and physical instabilities

The numerical simulation results of the 2D magnetically dominated bow shock flows presented in Chap. 6 were obtained with the Lax-Friedrichs flux function (see Sec. 4.2.5) on moderately fine grids. The resulting flow solutions are in a perfect steady state, and the physically consistent interpretation given validates the numerical results. However, we have found that various instabilities occur when we decrease the numerical dissipation further, by considering very fine grids or by employing less dissipative numerical flux functions, while keeping the simulation domain limited to the upper left quadrant. These instabilities may be of a numerical nature, or they may be caused by physical mechanisms, some of which may be related to the stability of shocks as discussed above. We have found that instabilities can change the flow locally while the global topology is conserved, and the flow can become intermittent or quasi-periodic, instead of stationary. It is often difficult to reach definite conclusions about the nature of instabilities in numerical results. In this Section we leave the discussion on MHD shock stability for a while and report on our experiences regarding these local instabilities. We attempt

to find explanations for the observed behavior of numerical methods and physical flows.

Failure of numerical schemes for bow shock flows

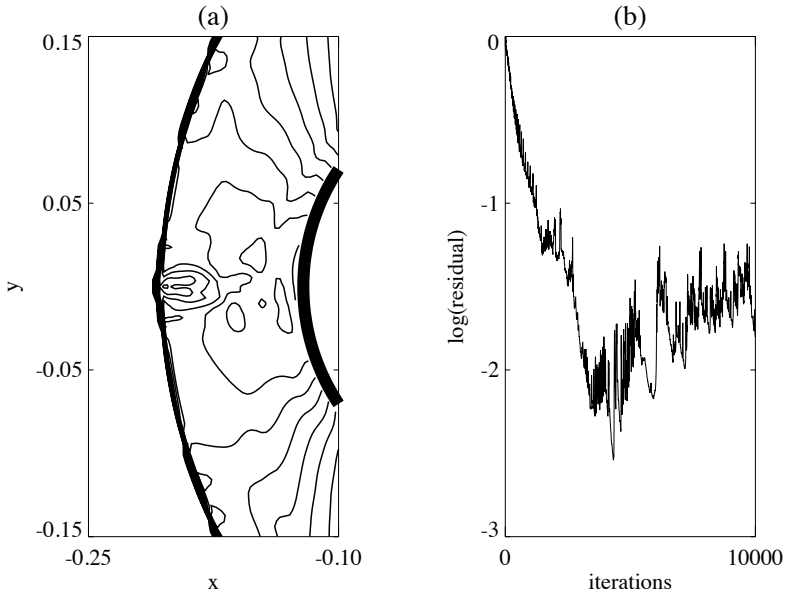

Figure 9.12: *Mach 10 hydrodynamic bow shock flow simulated using Roe's flux function. (a) The density contours show a deformation of the bow shock at the nose. (b) The solution is intermittent.*

It is well-known that numerical flux functions may suffer from various types of numerical instability problems [121, 108, 91]. In this Section we give some examples of the so-called carbuncle phenomenon, which is a well-known failure of many flux functions. For steady state, blunt body calculations the bow shock close to the stagnation line can be deformed, as can be seen in Fig. 9.12a for a Mach 10 hydrodynamic bow shock flow on a 100×201 grid simulated with our code using the second order scheme and Roe's flux function (see Sec. 4.2.5). The inflow quantities are $\rho = 1$, $p = 1$ and $v_x = 11.8$. Fig. 9.12b shows that the solution is intermittent and does not reach a steady state. The carbuncle effect appears to be more pronounced the more closely the grid is aligned to the bow shock, and for high Mach number flows. It is sometimes argued that this problem can be cured by applying the so-called *entropy fix*

to all the characteristic waves [121], but we have found that this does not help for high resolution simulations. The result in Fig. 9.12a is not perfectly symmetrical, although the initial and boundary conditions are symmetrical and this symmetry is conserved by the HD equations. This means that our code and the grid we use is not perfectly symmetrical (as in [121]). It is very hard to make a numerical code perfectly symmetrical, for instance because numerical operations are not fully associative up to the last digit on a computer. The order of computation is thus important, and compilers may change this order and may thus introduce a-symmetry in the process of optimizing the code.

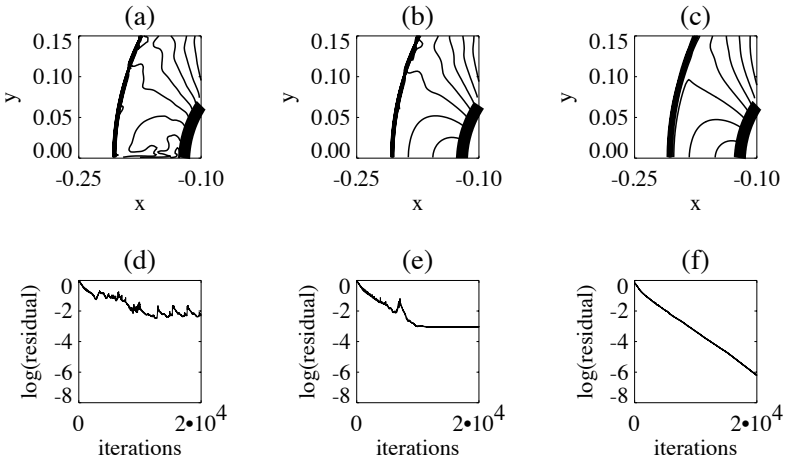

Figure 9.13: *Mach 10 hydrodynamic bow shock flows simulated in the upper left quadrant. Density contours and time convergence plots. (a,d) Roe. (b,e) HLLE. (c,f) LF.*

The bow shock flow simulations presented in Chap. 6 have been performed on a grid restricted to the upper left quadrant and with the symmetry explicitly imposed. The carbuncle phenomenon appears at the stagnation line in this configuration, as can be seen in Fig. 9.13a for simulation with the Roe flux on a 120×160 grid. The HLLE flux is known to be more robust [121, 99], and does not show the carbuncle in Fig. 9.13b, but the solution does not reach a steady state (Fig. 9.13e). The Lax-Friedrichs scheme (Fig. 9.13c and f) performs well due to its high and well-behaved numerical dissipation, but we are not aware of a proof that for very high grid resolution the carbuncle phenomenon does not appear.

Numerical dissipation

In general numerical instabilities are more likely to occur when the numerical diffusion is low or ill-behaved. Numerical diffusion is low on fine grids or for numerical flux functions which introduce a very small amount of diffusion for some characteristic waves. Some numerical flux functions introduce an ill-behaved numerical dissipation in the sense that the effective dissipation coefficient can become *negative*. This means that those numerical flux functions can *decrease* the entropy of fluid elements in numerically calculated flows. It is said that those numerical flux functions are not entropy consistent or not entropy stable [7]. The Roe scheme, for instance, is not entropy stable [7]. It follows clearly from the discussion on shock admissibility given above that an ill-behaved numerical dissipation may produce inadmissible shocks in numerical simulation results. For instance, for a negative value of the dissipative coefficient state -1 in Fig. 9.3 becomes unstable, and state 1 becomes stable, such that only shocks with diverging characteristics (Fig. 9.1a) would have viscous profiles! Expansion shocks can be produced by the Roe scheme [121]. An entropy fix is proposed to cure these problems with the Roe scheme [121, 90], but this fix does not cure all problems, like for instance the carbuncle phenomenon. The LF flux function has a well-behaved numerical dissipation, so we expect less influence from numerical instabilities. This was a motivation for the use of the LF flux function in the simulations presented in Chap. 6.

Decreasing the numerical dissipation in the 2D bow shock flow simulations

We now describe what happens when we substantially decrease the numerical dissipation for the bow shock flow simulation described in Sec. 6.2.

Let us first discuss simulations in which we used the Lax-Friedrichs flux function. The stationary simulation result discussed in Sec. 6.2 was faithfully reproduced on grids of size 60×60 to about 160×160. The solution has been reproduced with a different numerical code by Keppens *et al.* [83]. For finer resolutions, however, we have noticed some instabilities. In Fig. 9.14 we show the result of a simulation on a 320×320 grid. We have failed to obtain convergence to a perfect steady state, as can be seen in the convergence plot Fig. 9.14c. The solution is still close to a steady state though, and the fluctuations visible on time-animations of the solution are very small. Comparison of Fig. 9.14a with Fig. 6.9 shows some differences which can be interpreted as local instabilities, notably along the stagnation line, along the tangential discontinuity E–H, and near the intersection of the tangential discontinuity E–H with the intermediate shock D–G–H–I at point H. It is well-known that shear layers

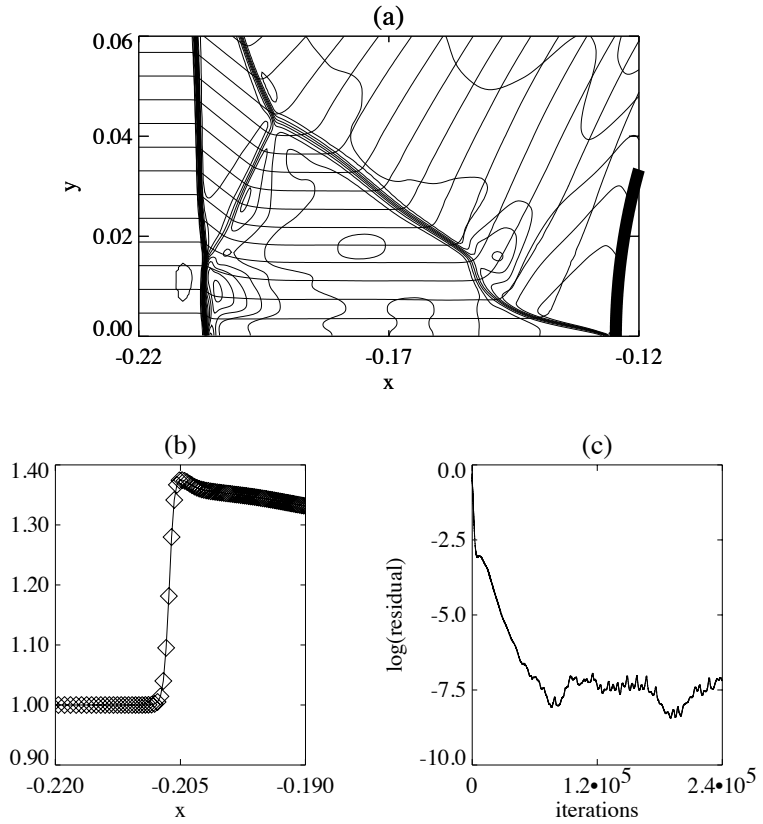

Figure 9.14: *LF simulation on a* 320×320 *grid. (a) Density contours and magnetic field lines. (b) Magnetic field profile along the stagnation line. (c) Convergence of the density residual.*

are physically unstable and show roll-up behavior, so this may explain the instability at the tangential discontinuity E–H. The instability on the stagnation line may be related to the numerical instability of carbuncle type discussed in the previous Section. The fact that the magnetic field is discontinuous in point F, as shown in Fig. 9.14b, seems to support this interpretation, because due to symmetry a continuous variation is required, as in the solution shown in Fig. 6.11d.

Regardless of these local instabilities and their nature, and regardless of the fact that the solution has become intermittent, we see that the flow retains the same general topology as the solution of Fig. 6.9. All the different segments of various MHD shock types are still present,

including the intermediate and compound shocks, so the analysis and interpretation given in Chap. 6 remains valid for flows with lower (numerical) dissipation.

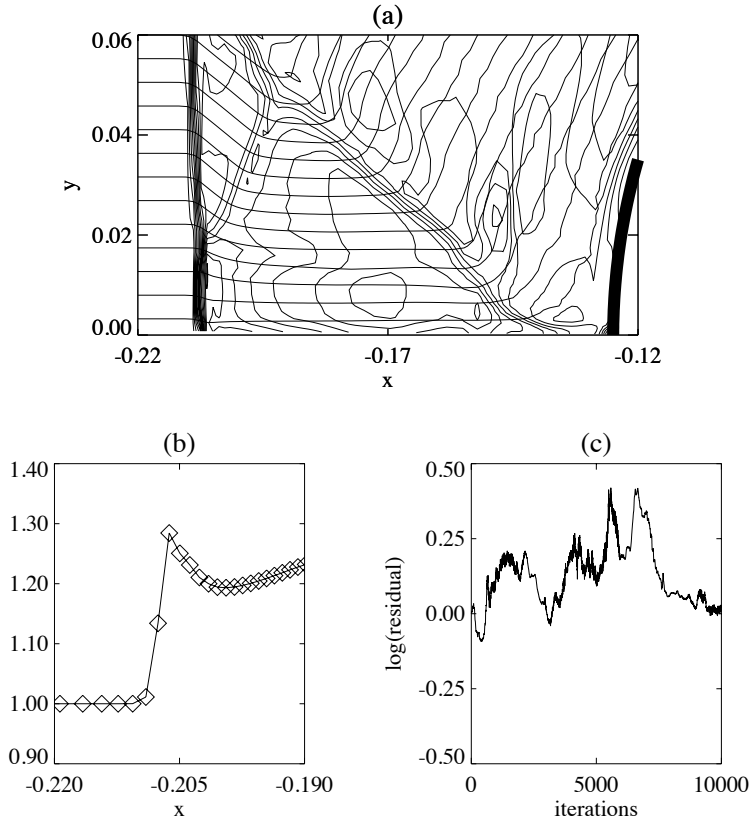

Figure 9.15: *Roe simulation on a* 80×80 *grid. (a) Density contours and magnetic field lines. (b) Magnetic field profile along the stagnation line. (c) Convergence of the density residual.*

Now we discuss the simulation results obtained with the Roe scheme and Linde's HLLE scheme. In Fig. 9.15 we show the result of a simulation on a 80×80 grid using Roe's scheme. This scheme has a lower and less well-behaved numerical dissipation than the LF scheme, and local instabilities already show up for coarse grids. This time the instabilities have a stronger influence on the temporal behavior of the solution. The residual fluctuates strongly and at high levels (Fig. 9.15c shows a part of the residual profile for a time interval well after the start of the sim-

ulation, and re-normalized to start with a value of zero), and animation of the simulation results shows strong fluctuations. Instabilities seem to be present at similar locations as in the case of LF simulations on fine grids. The instability at the stagnation line is probably a manifestation of the numerical carbuncle instability. We see an additional density layer at the ideal cylinder, which is probably related to the numerical effect of wall heating [90], a well-known defect of the Roe solver.

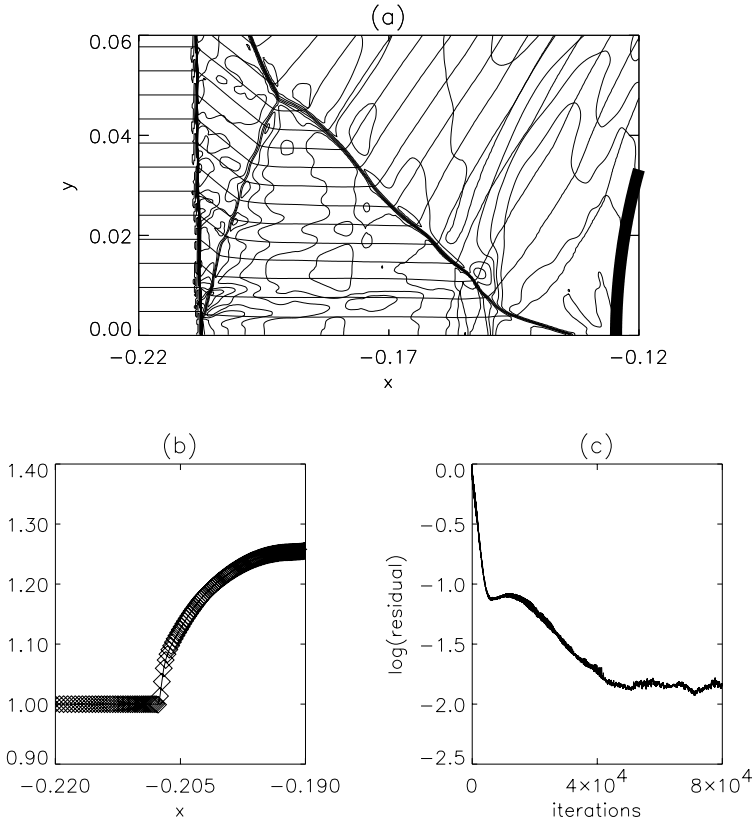

Figure 9.16: *HLLE simulation on a* 480×480 *grid. (a) Density contours and magnetic field lines. (b) Magnetic field profile along the stagnation line. (c) Convergence of the density residual.*

In Fig. 9.16 we show the result of a simulation on a 480×480 grid using Linde's HLLE scheme. This scheme is also much less dissipative than the LF scheme, so local instabilities show up quite strongly on fine grids. The instabilities again have a strong influence on the temporal

behavior of the solution. The residual fluctuates at high levels, and animation of the simulation results shows strong fluctuations. Instabilities seem to be present at similar locations as in the case of LF simulations on fine grids. The density is very oscillatory also away from the shocks, and this is due to the effect of entropy oscillations generated at the shocks — which are in a way too sharp — , which are transported along streamlines, as in Fig. 5.10a. This effect is much stronger on fine grids and for flux functions with low dissipation, like the HLLE flux function. The HLLE scheme seems to be remarkably robust against the carbuncle instability at point F, as the continuity of the magnetic field profile on the stagnation line proves. At point I, however, the solution is markedly different from the LF solution in Fig. 6.9. Also, the 1–4 shock segment E–F seems to become much smaller as point E migrates towards the stagnation streamline. This effect is investigated in more detail below. Wall heating effects seem not to be present in these HLLE simulations.

For both the Roe and the HLLE solver, the effects of the instabilities seem to be more severe than for the LF solver. However, the flow retains the same general topology as the LF solution of Fig. 6.9.

Stability of the 1–4 shock segment

We now look in some more detail at the behavior of the 1–4 shock segment for increasing grid resolution.

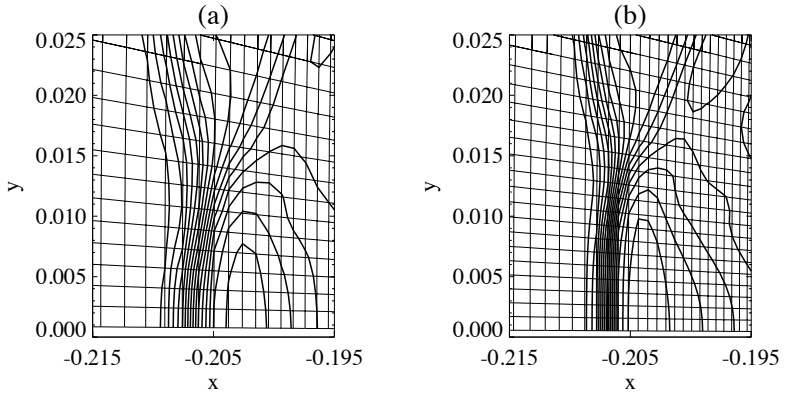

Figure 9.17: *Detailed representation of the 1–4 shock segment (density contours) near the perpendicular point F on the stagnation line, for LF simulations with different grid resolutions. (a)* 80×80 *grid. (b)* 120×120 *grid.*

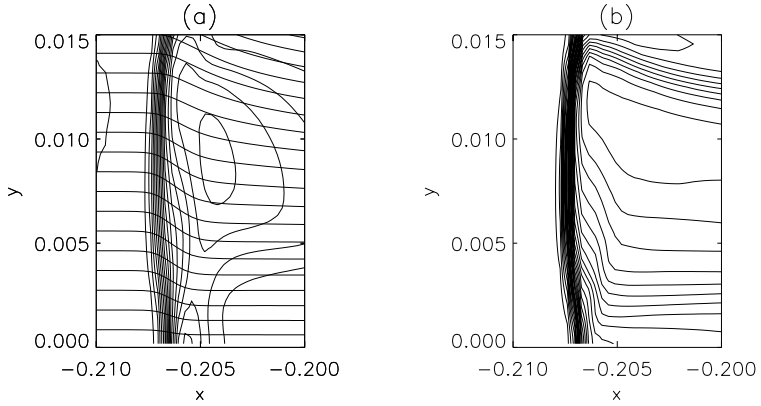

Figure 9.18: *Detailed representation of the 1–4 shock segment for LF simulation on a* 320×320 *grid. (a) Density contours and field lines. (b) Entropy contours.*

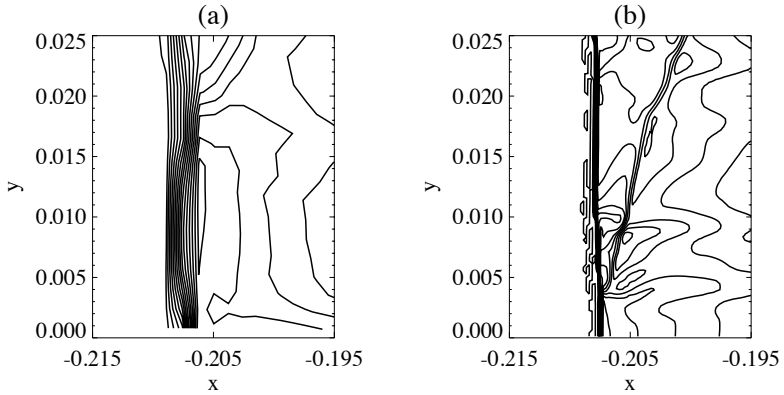

Figure 9.19: *Detailed representation of the 1–4 shock segment (density contours). (a) Roe on* 80×80 *grid. (b) HLLE on* 480×480 *grid.*

Fig. 9.17 shows detailed representations of this 1–4 shock segment for LF simulations with intermediate grid resolutions. The Figure shows that the 1–4 shock segment seems to be well-defined in the sense that it does not change its shape or extent when the grid is refined. However, in the LF simulation result with fine grid of Fig. 9.18, the 1–4 shock seems

to split up into two shocks.

Fig. 9.19 shows detailed representations of this 1–4 shock segment for the Roe and HLLE simulations presented above. The 1–4 shock remains intact for the Roe simulation on a 80×80 grid, but breaks down in the fine grid HLLE simulation such that point E moves much closer to the stagnation line. Close to the stagnation line, however, the 1–4 shock seems to remain intact. We have to admit that these results do not show much consistency. We can propose several possible explanations for the behavior of the 1–4 segment for increasing grid resolution. In Figs. 9.18 and 9.19b the 1–4 segment seems to split up into two shocks. This may be interpreted as supporting Falle and Komissarov's claim [35] that the 1–4 shock is non-evolutionary and should split up into two evolutionary shocks as the ideal MHD solution is approached by decreasing the dissipation. However, we have argued that a 1–4 shock can exist in ideal MHD flows. In simulations with numerical dissipation the 1–4 shock is stable against perturbations. Therefore we favor the following alternative interpretation for the breakup of the 1–4 shock. Physical or numerical instabilities, e. g. roll-up of the tangential discontinuity E-H or occurrence of the carbuncle instability at point F, may perturb the orientation of the 1–4 shock front EF. When in this process somewhere along the shock front EF the angle between the upstream magnetic field and the shock normal exceeds 3°, the shock front splits up (Fig. 3.10). Another possible explanation for the break-up in Fig. 9.19b is that the numerical dissipation of the HLLE scheme may not be well-behaved. It seems that high-resolution simulations of the MHD equations with a well-controlled small dissipation or with a code which does not introduce any numerical dissipation [35, 48] are needed to clarify the issue of the stability of the 1–4 front.

Comparison of the Powell technique and the projection approach

It is interesting to compare the Powell technique and the projection approach for the 2D bow shock flows and to verify if the approach used to control the $\nabla \cdot \vec{B}$ constraint (see Sec. 4.4) influences the stability of the solution.

Fig. 9.20 shows the comparison of LF flow simulation results on a 120×120 grid for simulation with the Powell source term (thin) and simulation with the projection scheme (thick), for various quantities along the stagnation streamline. First we can remark that the solutions are almost everywhere very close, so the two approaches both seem to produce valid results. Only near the stagnation point the results differ appreciably — see for instance the density in Fig. 9.20a. Then the question is which of the two results is more accurate. Fig. 9.20c shows that the

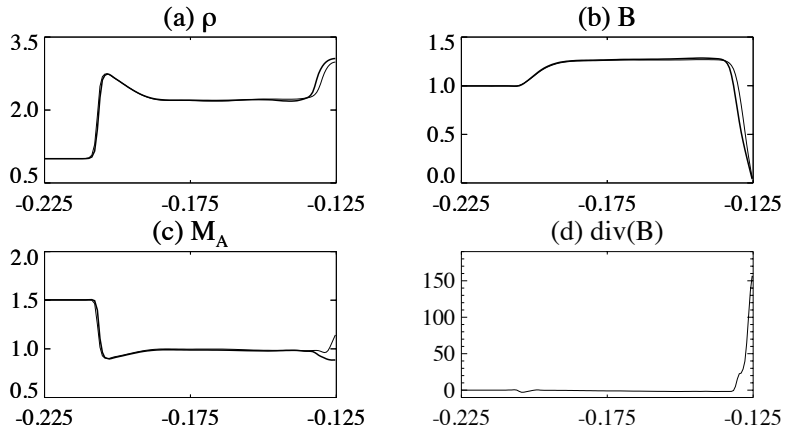

Figure 9.20: *Comparison of LF flow simulation results for simulation with the Powell source term (thin) and the projection scheme (thick), for various quantities along the stagnation streamline.*

Powell technique produces a solution for which the Alfvénic Mach number rises above one close to the cylinder. This is of course not physical, so the projection technique is more accurate. It is not unexpected that the Powell technique performs not so well at stagnation points, because the Powell technique can be interpreted as to advect $\nabla \cdot \vec{B}$ away with the flow. At a stagnation point the flow velocity vanishes, so $\nabla \cdot \vec{B}$ can accumulate. Fig. 9.20d shows that this is indeed the case ($\nabla \cdot \vec{B} = 0$ up to machine accuracy in our projection scheme approach). This accumulation of $\nabla \cdot \vec{B}$ leads to inaccuracies near the stagnation point, as the Powell technique is based on the cancellation of terms proportional to $\nabla \cdot \vec{B}$ on both sides of Eq. 3.12. Subtraction of two big numbers that are almost equal then leads to a high absolute error.

The projection scheme may thus lead to more accurate results in some cases, but still we have chosen to perform most simulations using Powell's technique, for several reasons. First, the Powell technique is much faster. Second, it can easily be parallelized, whereas the projection scheme necessitates the solution of a linear system in every time step, which is a non-local operation and thus hard to parallelize. Third, the solution of the elliptic projection equation introduces a coupling between all the points in the domain, and this may lead to contamination of upstream superfast regions which in theory should not be affected. Fourth, the projection scheme we use, like the schemes proposed in [129, 162, 161], leads to spurious modes due to odd-even decoupling. These oscillations are effectively damped out by the LF dissipation for the results shown

in Fig. 9.20, but on finer grids or for less dissipative flux functions the oscillations are much more pronounced.

9.4 Full MHD

9.4.1 Admissibility of shocks in full MHD

Shock admissibility

The 8×8 system of full MHD (Eq. 3.12) in one dimension has eight characteristic waves: two fast waves which propagate with speeds $v_x \pm c_{fx}$, two Alfvén waves with propagation speeds $v_x \pm c_{Ax}$, two slow waves with propagation speeds $v_x \pm c_{sx}$, and entropy and divergence waves which propagate with speed v_x (Eq. 3.35).

The full MHD system is non-strictly hyperbolic. In the direction parallel to the magnetic field the Alfvén speed c_{Ax} coincides with c_{fx} when $c_{Ax} > c$, or with c_{sx} when $c_{Ax} < c$. In each of these cases there are two degeneracies in which two characteristic speeds coincide. When additionally $c_{Ax} = c$, there are two degeneracies in which three characteristic speeds coincide, since $c_{fx} = c_{Ax} = c_{sx}$. In the direction perpendicular to the magnetic field c_{Ax} and c_{sx} vanish, such that the Alfvén and slow characteristic speeds coincide with the speed v_x of the entropy and divergence waves, implying a six-fold degeneracy.

The Alfvén waves are rotational waves of the type discussed in Sec. 9.2.4, and the full MHD system is rotationally invariant in the sense discussed in Sec. 9.2.4 [42, 46]. The fast and slow characteristic fields are non-convex, such that compound shocks can occur (see Sec. 3.3.5).

Some aspects of shock admissibility in the full MHD system are analogous to the case of the rotationally invariant and non-strictly hyperbolic system discussed in Sec. 9.2.4, but due to the many possibilities of multiple-fold degeneracies, the overall behavior is quite more complex.

Like in the planar case, for given shock speed s and flux constant vector $\mathbf{F}_{const}$ the RH relation 3.73 has up to four solutions which can be connected by shocks, labeled 1, 2, 3 and 4 in order of increasing entropy (Fig. 3.7). The shock admissibility in the full MHD system is, however, entirely different from the admissibility in the planar system, because rotational Alfvén waves exist which destabilize intermediate shocks.

Let us first consider the ideal system. Shocks which do not increase the entropy are undercompressive and thus non-evolutionary. Fast 1–2 shocks and slow 3–4 shocks are evolutionary and are thus admissible. All intermediate shocks (1–3, 1–4, 2–3 and 2–4) are overcompressive [87, 35]. According to the evolutionarity criterion they are inadmissible.

For the dissipative system, the dissipative parameters are the electric resistivity η, the thermal conduction κ, and two coefficients of viscosity

μ and ν [46]. Fast 1–2 shocks and slow 3–4 shocks have unique viscous profiles for all values of the dissipative parameter vector $\delta = (\eta, \kappa, \mu, \nu)$. All intermediate shocks do not have viscous profiles for some range of δ, with this range depending on the shock type and the left and right states. All intermediate shocks do have viscous profiles for some range of δ. This has been proven in [49], where it is shown that the profiles are generated in a global heteroclinic bifurcation controlled by ratios of the dissipative coefficients. Good numerical illustrations of the effect of this bifurcation for MHD flows can be found in [173].

When profiles exist for intermediate shocks, they generally are not unique but are members of families of profiles. As shown in Sec. 9.2.4, this allows the overcompressive intermediate shocks to be conditionally stable against Alfvénic perturbations which introduce magnetic field out of the plane of coplanarity of the shock. The quantity $I_z = \int B_z \, dx$, with z the direction out of the plane of coplanarity, x the direction perpendicular to the shock front and integration over the length of the shock profile, plays an important role in the stability of intermediate shocks [173, 109]. For a given intermediate shock — left and right states satisfying the RH relations — and for a given value of δ for which the shock can have viscous profiles, a shock profile can exist only if the weight I_z of B_z in the profile is smaller than a certain I_z^{crit}. When the shock is perturbed — for instance by sending in an Alfvén wave packet — I_z builds up in the shock profile, until it exceeds the critical value and the shock splits up in other waves. The stability is non-uniform in the magnitude of the dissipation, in the sense that the critical value I_z^{crit} vanishes for vanishing δ with constant $\delta/||\delta||$ [46, 47]. This resolves the contradiction between the fact that intermediate shocks are inadmissible in the ideal system, but have viscous profiles in the dissipative system. Dissipative MHD thus approaches ideal MHD for vanishing dissipation. Vanishing viscosity limits are not uniform and are not unique because the existence of intermediate shocks in solutions depends on ratios of dissipative coefficients.

The dissipative system does thus not *uniformly* approach the ideal system for vanishing dissipation. One manifestation of this is that shock admissibility is different for the ideal and the dissipative systems. This implies that shock admissibility criteria from the ideal system cannot simply be used to determine admissibility of dissipative shocks — what Falle and Komissarov [35] apparently try to do —, and vice versa, that dissipative criteria cannot simply be used to determine admissibility of ideal shocks — what Myong and Roe [109, 110] apparently try to do. For strictly hyperbolic systems like the HD equations, ideal admissibility criteria can be applied to the dissipative system and vice versa. For MHD this is not true, and it seems that much of the confusion in the literature on the admissibility of MHD shocks stems from attempts to

apply dissipative criteria to the ideal system [109, 110] or the other way around [35]. It has been argued that dissipative criteria can be used to determine admissibility of ideal shocks if one considers waves that are non-uniformly stable in the dissipation inadmissible in the ideal system, while considering uniformly stable waves admissible [102]. Indeed, dissipative and ideal MHD do approach each other, but the non-uniformity has to be taken into account.

Riemann problems

The non-uniformity of vanishing viscosity limits can be illustrated by considering Riemann problems, analogous to the Riemann problem for the rotationally invariant model problem which was discussed in Sec. 9.2.4. Fig. 9.21 shows a solution of the Riemann problem introduced by Brio and Wu [12] obtained by our numerical code. A slow compound shock arises in the solution. The 2–3=4 sonic intermediate shock is admissible in the dissipative system, so our numerical code with numerical dissipation produces a solution with the compound shock. We have performed the simulation in full MHD, so Alfvénic perturbations due to non-perfect symmetry of the code would destroy the shock if it were generically unstable. Such small perturbations of B_z do indeed arise, but the shock clearly persists. In the ideal system, intermediate shocks are not admissible. Rotational Alfvén waves destabilize intermediate shocks, and at the same time provide a different way of changing the sign of the tangential magnetic field component. A rotational discontinuity thus takes over the role of the compound shock in the ideal solution of the Riemann problem. Falle and Komissarov indeed produce this ideal solution with their dissipation-free numerical code based on the Glimm scheme [35].

It seems that the fact that numerical codes with or without numerical dissipation produce different solutions to this Riemann problem is thus satisfactorily explained by the above observations. Some authors still seem to think that the existence of two solutions is a problem, and claim that one of the two is the only valid solution. Falle and Komissarov [35] argue that the solution with the rotational discontinuity is 'the only physically admissible solution to the Riemann problem'. This is of course not true. Their claim is probably true if they were to restrict it to the ideal MHD system (which they do not!), but in the dissipative MHD system the solution with the compound shock is certainly admissible! Even in the limit of vanishing dissipation — equivalent to refining the grid in a code which employs numerical dissipation — the solution of this problem is the compound shock solution [48]. Myong and Roe [109] claim that intermediate shocks are 'physical'. They argue that intermediate shocks are admissible in full MHD, and can thus arise in Riemann

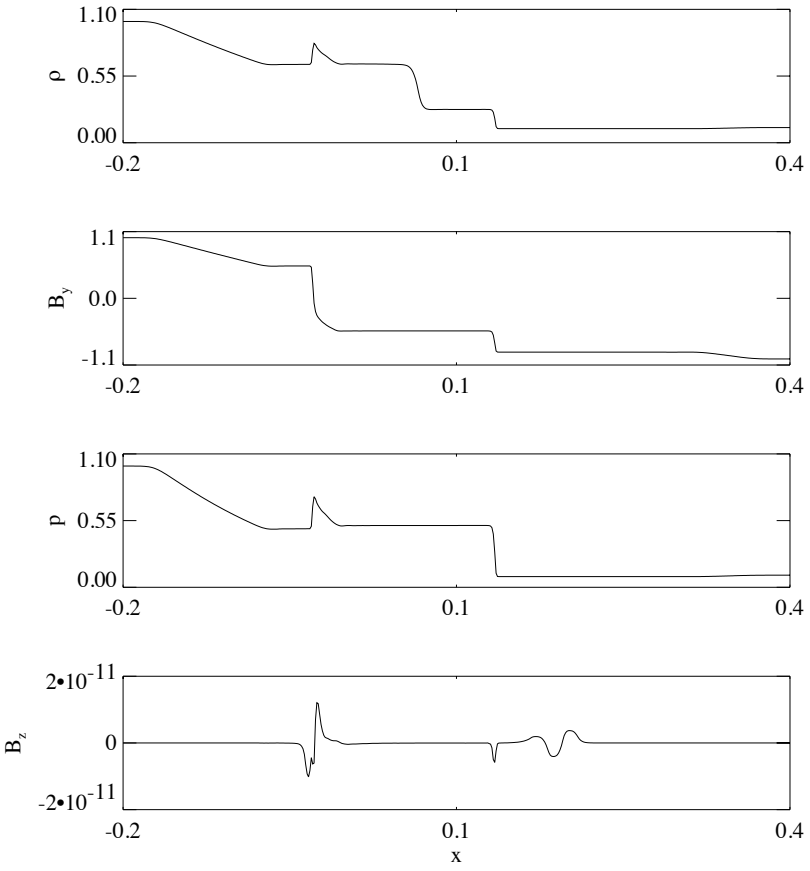

Figure 9.21: *Riemann problem solution. The density, the pressure, the tangential component B_y of the magnetic field in the plane of coplanarity and the component B_z out of this plane are shown. The following waves can be identified (from left to right): a fast rarefaction, a slow compound shock (a sonic slow shock with an attached rarefaction), a contact discontinuity, a slow shock and a fast rarefaction.*

problem solutions. This claim would be true if they were to specify that they talk about the dissipative system only (which they do not specify!). In solutions of the ideal system intermediate shocks can probably not arise. We can thus conclude that if controversy remains, this is mainly due to the fact that some authors do not precisely formulate the range of validity for their claims or, equivalently, do not specify precisely what they mean by 'physically admissible'. We come back to the question of

'physical admissibility' in Sec. 9.4.3.

Time-dependent intermediate shocks

Due to the non-strictly hyperbolic nature of MHD, the dissipative MHD system allows for the peculiar phenomenon of *time-dependent intermediate shocks* [173, 178, 177]. This phenomenon has no analogy in HD flow.

In the strictly hyperbolic HD system, an initial discontinuity which does not satisfy the RH relations — this is the initial condition of a Riemann problem — splits up in waves which each satisfy the RH conditions and move with the shock speeds dictated by the RH relations. This is true for both ideal and dissipative HD. In dissipative HD the shocks have unique viscous profiles.

In the dissipative MHD system, however, an initial discontinuity which does not satisfy the RH relations splits up in waves of which some may be compressive waves which do not satisfy the RH conditions. In these compressive waves dissipation balances compressional steepening — characteristics converge into the wave — and they thus have a profile of limited spatial extent. The flow is sub-Alfvénic upstream and sub-Alfvénic downstream. These waves are called time-dependent intermediate shocks. The profile of waves that do not satisfy the RH relations necessarily undergoes a change in time. This can be seen by integrating the conservation law over the length of the profile in the frame moving with the wave. For a wave satisfying the RH relations we find that $\partial(\int u\,dx)/\partial t = f(u_r) - f(u_l) = 0$, while for a wave not satisfying the RH relations the weight $\int u\,dx$ of the profile has to change in time according to $\partial(\int u\,dx)/\partial t = f(u_r) - f(u_l) \neq 0$. We propose the conjecture that this continuous change in profile is possible in MHD because intermediate shocks have *families* of viscous profiles, whereas in the HD system shocks have *unique* profiles and time-dependent shocks do not occur in 1D Riemann problems. In dissipative MHD, time-dependent intermediate shocks arise in the solution of non-coplanar Riemann problems. They do not move with constant speed. For large times they evolve to non-intermediate discontinuities which satisfy the RH relations.

In ideal MHD time-dependent intermediate shocks cannot occur because ideal discontinuities do not have a profile and thus necessarily have to satisfy the RH relations! Solutions of non-coplanar Riemann problems do not contain any intermediate shocks, but instead they contain from the start the shocks which appear in the dissipative solution for large times.

9.4.2 Shock types in 3D magnetically dominated bow shock flows

Intermediate shocks have to our best knowledge previously not been observed in 3D MHD simulations.

The magnetically dominated bow shock flows around spheres that were presented in Chap. 7 (e.g. Fig. 7.1) clearly show the presence of stationary intermediate shocks of 1–3 and 2–4 types. The necessary presence of intermediate shocks in the bow shock topology for the magnetically dominated parameter regime is confirmed by reasoning based on the geometric properties of MHD shocks (Fig. 7.5b). A 1–3 shock segment arises in the leading shock front of the flow of Fig. 7.1, and the secondary front is of 2–4 type (Figs. 7.10 and 7.8).

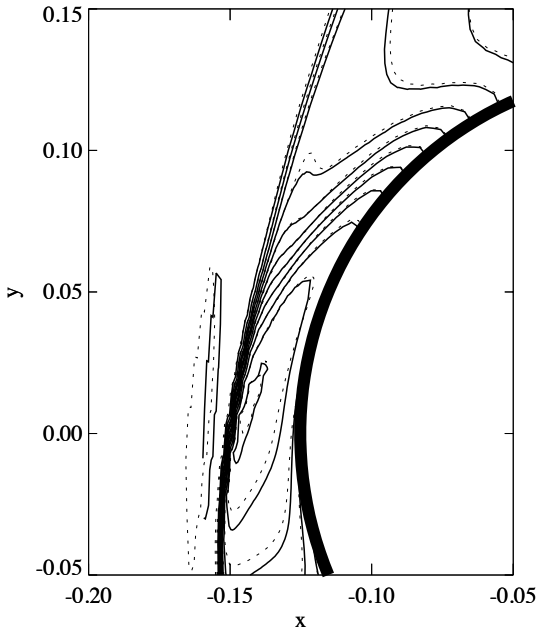

Figure 9.22: *Bow shock simulation results in the xy plane for the parameters of Fig. 7.1, on a randomly perturbed* $60 \times 80 \times 80$ *grid covering the half space on the upstream side of the sphere (solid), and on a symmetrical* $60 \times 60 \times 40$ *grid covering the upper upstream quadrant (dotted). The two solutions agree, thus the solution containing 3D intermediate shocks is stable against non-symmetrical grid perturbations.*

Falle and Komissarov [35] argue that intermediate shocks can sometimes 'pollute' full MHD flows due to artificial symmetry. One could argue that the simulation result of Fig. 7.1 contains artificial symmetry because we have performed the simulation only in the top left quadrant and we explicitly impose the symmetry at the xy plane. Uniform MHD flow around a sphere always has such a plane of symmetry, however. This symmetry is intrinsic to the physical problem, and is thus not artificial. We have verified if the intermediate shocks remain present in the bow shock flow solution when the symmetry at the xy plane is not perfectly imposed. To this end we have simulated the bow shock flow of Fig. 7.1 on a randomly perturbed grid covering the half space on the upstream side of the sphere, and not just the upper upstream quadrant. Fig. 9.22 shows that the solution with intermediate shocks survives when we perturb the symmetry of the xy plane slightly by perturbing the grid. The two solutions in Fig. 9.22 agree, thus the solution containing 3D intermediate shocks is stable against non-symmetrical grid perturbations.

Fig. 7.20 shows that compound shocks can arise in 3D simulations of the full MHD system. Falle and Komissarov [35] claim that full MHD is effectively convex and that compound shocks cannot arise in full MHD flows. Again, there claim may be justified for the ideal MHD system, but is clearly false in the general way they put it, because compound shocks can arise in full MHD flows with small dissipation.

In brief, our simulation results of 3D bow shock flows show that in physically realistic flows described by full MHD with small dissipation intermediate shocks can exist and persist.

9.4.3 Physical admissibility of intermediate shocks

Are intermediate shocks physical?

Intermediate shocks are physical if they can be observed in plasmas in nature. It seems justified to suppose that dissipative processes are active in some way in all plasmas in nature. These dissipative processes do not necessarily have to be of a collisional nature, but may be due to microscopic particle-wave interactions and instabilities. Let us thus assume that all physical plasmas undergo some kind of dissipation. Let us further assume that MHD is a good description of shock phenomena in plasmas. This is not entirely obvious, and we refer the reader back to Sec. 2.3.1 for some thoughts on this issue. Under these assumptions we can say that intermediate shocks are physical if they can arise in solutions of the full MHD equations with small dissipation.

The discussion in Sec. 9.4.1 has shown that intermediate shocks are admissible in full MHD for large ranges of the dissipative parameters. Our 3D simulation results of bow shock flows have shown that intermediate shocks can be formed and can persist in realistic MHD flows

with small dissipation. We thus conclude that intermediate shocks are physical.

It is probably true that intermediate shocks cannot arise in *ideal* MHD flows. But this does not mean that intermediate shocks are unphysical, because all plasma flows are presumably subject to dissipation and ideal MHD is in some sense not a good description of small dissipation MHD.

Falle and Komissarov [35] indeed agree that intermediate shocks 'may, perhaps, appear under some exceptional circumstances as transient phenomena' (at which point we have to assume that they speak in the context of dissipative MHD, although again this is not clearly specified). It then seems unjustified that they keep on calling intermediate shocks 'unphysical'. The reason why they still do so, is their claim that in any physical system intermediate shocks can never exist long enough to be observed, because existing intermediate shocks would supposedly be destroyed by small Alfvénic perturbations. They argue that the amplitude of Alfvénic perturbations necessary for destroying intermediate shocks is very small in space plasmas because the dissipation is very low. They give the example of interplanetary intermediate shocks traveling in the solar wind. Chao [18] claims the observation of an interplanetary intermediate shock by the Voyager 1 spacecraft. Falle and Komissarov [35] argue that when an intermediate shock would travel from the sun in the direction of a satellite, Alfvénic perturbations in the solar wind would destroy the intermediate shock before it can reach the satellite. This may be true, but does in our opinion not mean that intermediate shocks cannot be observed in other physical contexts.

Indeed, Falle and Komissarov [35] never consider how intermediate shocks can be *formed* in space plasmas. Their reasoning is based on physical intuition which stems from considering 1D Riemann problems. Riemann problems are artificial in a sense, because the initial state is given as such and has not been formed by physical processes. Once shocks are destroyed by perturbations, there is no driving mechanism to reform them. When a certain symmetry or coplanarity is present in a given Riemann problem, it can always be argued that the symmetry is arbitrarily imposed and that Riemann problems with symmetry do not constitute generic cases [35]. The shocks arising in these symmetrical or coplanar cases are then considered artificial too, and it is easily concluded that these 'exceptional' shocks do not arise in 'generic' physical flows. These interpretations are based on physical intuition stemming from Riemann problems. In the literature shock admissibility is almost always discussed in the context of 1D Riemann problems. This context is not necessarily the most physically relevant. For instance, perturbation of the left or right states of a Riemann problem implies a perturbation with an unbounded weight I_z, which certainly is not the only physically

relevant way of perturbing a shock. We think that a different and more pertinent physical intuition is provided by considering *driven* problems in multiple dimensions.

The bow shock flows we have discussed in Chaps. 6 and 7 are *driven* problems in which shocks are formed by physical processes. When shocks are destroyed by perturbations, they can possibly be reformed. The bow shock flows possess an intrinsic symmetry due to the physical nature of the problem. In the case of 3D flow over a sphere the uniform inflow can be changed — for instance by rotating the magnetic field vector around the velocity vector — such that the plane of symmetry of the solution ceases to be a plane of symmetry, but by the physical nature of the problem the new inflow defines a new plane of symmetry! The bow shock flows are 2D and 3D. In 2D and 3D geometrical constraints can arise which necessitate the occurrence of certain shocks like switch-on shocks and intermediate shocks. For instance, the reasoning leading to the topology of Fig. 7.5b was clearly based on such constraints. These constraints do not arise in 1D Riemann problems.

The physical nature of driven problems in multiple dimensions is thus entirely different from the nature of 1D Riemann problems. In contrast to the conclusions often derived from considerations in the context of Riemann problems, we conclude from our simulation results of driven bow shock problems that intermediate shocks can be formed and can persist in physically relevant flows. If they are destroyed by perturbations, they can be reformed by the same process by which they were formed initially. The symmetry or coplanarity required for this reformation is intrinsic to the physical nature of realistic driven problems in multiple dimensions. This indicates that intermediate shocks are physical and can be observed. They may even be observable as close to the earth as in the bow shock formed in front of the earth by the solar wind when the solar wind is magnetically dominated! The 4 CLUSTER satellites, planned to be launched by mid-2000, may be able to detect a 1–3 intermediate shock segment in the earth's bow shock under magnetically dominated solar wind conditions.

On the relevance of ideal MHD

The discussion above raises questions about the relevance of ideal MHD for the description of real plasmas.

In their writing Falle and Komissarov [35] seem to claim implicitly that ideal MHD can be used to describe real plasmas because the differences between ideal and dissipative MHD are considered small and not observable because of omni-present small perturbations.

In contrast, Wu [173] argues strongly against the use of ideal MHD to describe real plasmas. He claims that 'whenever a rotation of the

magnetic field occurs, (ideal MHD) is not a good approximation to dissipative MHD'. He argues that small dissipation MHD is the physically relevant case, and that ideal MHD is not a good description of small dissipation MHD. He shows that solutions to Riemann problems critically depend on shock profiles, on the nature of the dissipation mechanism, and on the magnitude of the dissipative parameters. Ideal MHD can clearly not describe these aspects of small dissipation MHD flows. Wu even seems to imply that ideal MHD is not a valid or consistent theory. He argues that the ideal Riemann problem is not well-posed, because a given Riemann problem can have many different solutions.

Freistuehler [45] states that the fact that intermediate shocks are not admissible in ideal MHD while they can be admissible in dissipative MHD, 'shows severe limitations of ideal MHD in its role as a model of small dissipation MHD. On the other hand, these limitations are non-uniform themselves and they will not make ideal MHD completely useless for *physical* interpretation whenever discontinuities are present. Certainly, they do not preclude *mathematical* self-consistency of ideal MHD.' Freistuehler argues that 'ideal MHD has a self-consistent theory in which intermediate shocks do not occur' [46], although he does not prove this. The objection of Wu against ideal MHD, namely that ideal MHD is ill-posed because Riemann problems can have multiple solutions, is neutralized by arguing that of these many solutions only the one without intermediate shocks is admissible in ideal MHD.

The picture sketched by Freistuehler seems the most attractive. Ideal MHD is well-posed and has a self-consistent solution theory. Ideal and dissipative MHD do approach each other for small dissipation, so ideal MHD can describe flows with small dissipation up to a certain extent. However, they do not *uniformly* approach each other. For instance, intermediate shocks can exist in dissipative MHD, but not in ideal MHD. Therefore detailed description of some phenomena in real (dissipative) plasmas requires dissipative MHD with precise control of the mechanism and magnitude of the dissipation.

On the relevance of shock-capturing numerical techniques for non-strictly hyperbolic systems

Freistuehler's [48] and Wu's [173] work implies that in numerical simulations dissipation mechanisms and magnitudes have to be specified precisely and that shock profiles have to be resolved in order to be able to properly describe some shock phenomena in real MHD plasmas with dissipation.

Such a numerical approach is entirely opposite to the approach generally followed for the simulation of flows with shocks described by strictly hyperbolic systems like the HD equations. Indeed, in modern *high-*

resolution shock capturing codes [90] one discretizes the ideal equations, and one aims at minimizing the numerical dissipation in order to approach as closely as possible the dissipation in the physical system, which is often much lower than the attainable minimum numerical dissipation. Shock profiles are typically not resolved, but one aims at reducing the shock width to a minimal number of computational cells. Can these shock-capturing numerical techniques be used for the simulation of flows with shocks described by non-strictly hyperbolic systems?

It would obviously be better to discretize the dissipative terms and to resolve shock profiles. However, this approach requires much larger computer resources. For some problems, like the study of the detailed interaction of an Alfvén wave with an intermediate shock, this may be required, but for other problems less computationally intensive methods may suffice. When intermediate shocks do not arise — in pressure-dominated flows with high upstream plasma β for instance —, shock-capturing methods can safely be used. When intermediate shocks arise shock-capturing methods may still produce relevant results in the following sense. First of all it seems essential that the numerical dissipation is well-behaved. This is generally required for any numerical method and any flow problem, but seems extremely important for the stability of intermediate shocks. The topology of flow solutions depends on the existence of intermediate shocks, which in turn depends on the values of the dissipative parameters. The existence of intermediate shocks is controlled by bifurcation. For large ranges of the dissipative parameters the existence properties of intermediate shocks do not change. This means that flow solutions of a given problem come in classes with the same topology for large ranges of the dissipative parameters. A flow solution obtained by a shock-capturing code with well-behaved numerical dissipation can thus be expected to be generic for large ranges of the dissipative parameters. Such a solution is presumably physically relevant, especially in the case of steady problems without dynamical perturbations. When perturbations and small-time behavior are important in the problem, however, the dissipation mechanism should be specified and shock profiles should be resolved. It has to be admitted that dissipation mechanisms and magnitudes are often not well known for space plasmas or cannot be simulated because the numerical dissipation necessary for stability is much larger. In such cases the use of shock-capturing codes with a well-behaved numerical dissipation may be justified.

Vanishing viscosity limit and ideal solution for the 3D magnetically dominated bow shock flows

The 3D simulations of magnetically dominated bow shock flows that were described in Chaps. 7 and 8 were performed with a shock-capturing

numerical code. They are solutions of the MHD equations with a certain unspecified (numerical) dissipation. We did not observe a change in flow solution when we varied grid sizes. We expect that the topology obtained has some general validity for a large range of the dissipative parameters. This should be verified by repeating the calculations for various sets of dissipative parameters with a code which discretizes the dissipative terms and resolves shock profiles.

It is an interesting question what the vanishing viscosity limit solution of these magnetically dominated bow shock flows (e.g. Fig. 7.1) would be. This could be investigated by refining the grid in simulations with a shock-capturing code. We anticipate that in the symmetry plane (xy) the topology would not change, because the reasoning which lead to the topology of Fig. 7.5b and to the break-up of the 1–3 shock at a certain critical angle is independent from the dissipation. The extent of the secondary shock out of the xy plane could possibly depend on the magnitude of the dissipation, but most probably it is also determined by geometrical constraints which do not depend on dissipation. The topology of Fig. 7.1 may thus be the topology of the vanishing viscosity solution.

Another interesting question is what the ideal solution to this flow problem would be. The ideal solution would presumably not contain intermediate shocks [46]. The 1–3 shock segment in the topology of Fig. 7.5b would presumably break up in a fast 1–2 shock followed by other waves. A 3D code without numerical dissipation would be required to investigate this. Numerical investigation of this problem seems to be a daunting task.

We may not exclude the following possibility, however. The conclusion that intermediate shocks are inadmissible in ideal MHD was reached based on stability study in one spatial dimension. The ideal MHD system is strongly degenerate as is for instance clear from the fact that wave speeds can coincide in multiple ways. It is possible that some of the degeneracies are lifted in 2D or 3D and that intermediate shocks would turn out to be admissible in ideal MHD in 2D and 3D. If so, then the topology of Fig. 7.1 may be the topology of the ideal flow solution. The reasoning leading to the topology of Fig. 7.5b is indeed convincing, and it seems not immediately clear why it should not be valid for ideal MHD. The geometrical properties of MHD shocks seem to require the presence of 1–3 intermediate shocks on the leading shock front of a 3D bow shock flow for magnetically dominated upstream parameters, and this could be so also in the ideal MHD case. Study of shock stability beyond the 1D approach has only briefly been touched upon in the literature [105]. The theoretical study of shock stability in multiple dimensions has recently been begun [184].

9.5 Conclusion

We have shown how the planar 2D magnetically dominated bow shock flows around cylinders that were discussed in Chap. 6 form excellent illustrations in 2D of the theory on the admissibility of shocks in planar MHD. The 3D magnetically dominated bow shock flows around spheres that were discussed in Chap. 7 were shown to be excellent illustrations in 3D of the theory on the admissibility of shocks in full MHD. Intermediate shocks had been found previously in 1D and in some 2D simulation results, but the bow shock flows described in Chaps. 6 and 7 are the first clear illustrations in 2D and 3D of the whole variety of intermediate shock phenomena that can arise in MHD flows.

Some authors argue that intermediate shocks cannot be observed in physical systems [107, 35]. Our simulation results of driven bow shock flow problems indicate that intermediate shocks can be formed and can persist in physically relevant flows with small dissipation. Intermediate shocks should thus be observable in physical plasmas.